Deep Resources Engineering 1 (2024) 100020

Contents lists available at ScienceDirect

Deep Resources Engineering

journal homepage: www.keaipublishing.com/en/journals/deepre/

Review

Advances in dynamic test of deep rocks considering in-situ mechanical and hydraulic conditions

Kaiwen Xia [a,b,*], Minlei Wang [b], Yan Fu [b], Bangbiao Wu [b], Ying Xu [b], Wei Yao [b,**]

[a] Institute of Geosafety, China University of Geosciences (Beijing), Beijing 100083, China
[b] State Key Laboratory of Hydraulic Engineering Intelligent Construction and Operation, School of Civil Engineering, Tianjin University, Tianjin 300072, China

ARTICLE INFO

Keywords:
Deep rock dynamics
Triaxial confinement
Hydraulic-mechanical coupling
Dynamic strength
Dynamic fracture toughness

ABSTRACT

Determining the dynamic behaviors of deep rocks is important but challenging for deep underground rock engineering. Recently, great advances have been made by researchers in dynamic tests of deep rocks considering in-situ mechanical and hydraulic conditions. It is thus imperative to systematically review the progress in this field. This paper focuses on the dynamic experiments of deep rocks using the modified split Hopkinson pressure bar (SHPB), including new advances in experimental apparatuses, methodologies, and results. A comprehensive introduction to the principles of the triaxial confinement SHPB, the true triaxial SHPB, and SHPB with a coupled hydraulic-mechanical device is provided. The development of these systems for conducting dynamic tests of deep rocks is briefly presented. Moreover, the experimental methods and results for quantifying dynamic compressive, tensile, flexure, and shear strengths and mode I/II fracture toughness of rocks under axial preload, hydrostatic pressure, triaxial stress state, and coupled hydraulic-mechanical condition are systematically discussed, and the rate-dependent characteristics and mechanisms of deep rocks under various geological occurrence conditions are also summarized.

1. Introduction

As shallow resources are nearly exhausted, mining and civil operations are bound for deeper underground. Deep underground rock engineering is generally at depths of 1000 ~ 2000 m [1]. For example, the depth of the Sangzhuling tunnel in China is 1347 m [2]and the maximum depth of the Yigong tunnel in China is 1610 m [3,4]. The depth of the Jinping II hydropower station on the Yalong River reaches 2500 m [5]. The depth of Motuo Hydropower Station on the Yarlung Zangbo River is up to 4000 m. Deep rock engineering is also closely related to the disposal of nuclear waste [6,7] and geothermal extraction [8], etc. The exploitation of the deep resources and energy is challenging as the deep rocks experience extremely complex stress conditions, under which the mechanical response of rocks may significantly differ from that in the shallow earth. Deep rocks are generally subjected to a complex geological environment with high in-situ stress, high differential pore pressure, high temperature, and dynamic disturbances caused by operational blasting and earthquakes. Therefore, understanding the dynamic mechanical properties of rocks under deep geological conditions is essential for revealing the dynamic failure mechanism of deep rocks and further guaranteeing the safe exploitation of deep resources and energy.

The high in-situ stress, high temperature, and high pore pressure are the basic attributes of deep rock engineering, and the thermal-hydraulic-mechanical coupling behaviors under such geological environments have attracted great attention worldwide in recent years [1,5,9–13]. Deep rocks exhibit unique characteristics of crack propagation, fluid inrush, unloading fragmentation, and rheological behavior when the depth of rock engineering activities extends 1000 m due to the high in situ stress state (Fig. 1 [14,15]). For instance, during the tunneling excavation of the Jinping II Hydropower Station at a depth of 2500 m, rockbursts occurred frequently in the surrounding rock masses, and the frequency and intensity of the rockbursts increase with the depth of the tunnel [5,13,16]. Furthermore, the mechanical properties of deep rock masses are also influenced by the coupling effects of multiple physical fields such as temperature, pressure, and pore pressure. The gradients of geothermal engineering can reach 30–50 °C/km [17]. Meanwhile, when the burial depth exceeds 1000 m, water pore pressure in deep rock masses can reach up to 7 MPa, potentially inducing severe water inrush accidents during excavation. Furthermore, the dynamic disturbances

* Corresponding author at: China University of Geosciences (Beijing), Beijing 100083, China.
** Corresponding author.
E-mail addresses: kaiwen.xia@cugb.edu.cn (K. Xia), yaow@tju.edu.cn (W. Yao).

https://doi.org/10.1016/j.deepre.2024.100020
Received 1 May 2024; Received in revised form 14 May 2024; Accepted 14 May 2024
Available online 18 May 2024

induced by the fault activation, blasting operation, or periodic roof weighting would increase the possibility and frequency of deep geological disasters (e.g., earthquake, rockburst, coal and gas outburst, etc.). Therefore, it is imperative to develop an effective experimental system to explore the dynamic mechanical properties of rocks under deep geological conditions.

The stress wave propagation in deep rocks [18,19] and the dynamic response of deep rocks [1,20] are two primary issues in deep rock dynamics. For the dynamic response of deep rocks, many scholars have summarized the existing research results and the key scientific issues [1, 20–23], and found that laboratory experiments are effective methods to obtain the dynamic responses of deep rocks. Laboratory experimental devices commonly include plate impact experimental devices, light gas gun, drop weight, and split Hopkinson pressure bar (SHPB). Due to the reliability and variability, SHPB has been extensively modified to qualify the dynamic compressive, tensile, shear, and fracture behaviors of rock-like materials, and some scholars have systematically summarized and reviewed the principles and methodologies of various modified SHPB systems and the experimental results derived from these systems [24–29]. However, the experimental methods and the experimental results abovementioned are only focused on shallow rocks. Therefore, several researchers developed novel SHPB systems that can be used to meet the experimental needs of deep rock dynamics [30–37]. This paper systematically summarizes the principles and methodologies of the modified SHPB system for deep rocks and the experimental results of the dynamic mechanical properties of rocks under deep geological conditions.

After the introduction, the principles of the triaxial confinement SHPB system are systematically described and the experimental results of dynamic mechanical properties of deep rocks under triaxial confinement are discussed in detail. In Section 3, the structures of the true triaxial SHPB system and the dynamic behaviors of rocks under true triaxial stress states are reviewed. SHPB with a coupled hydraulic-mechanical experimental device and the dynamic mechanical and transport properties of deep rocks are introduced in Section 4. Finally, the conclusions are drawn in Section 5.

2. Triaxial SHPB system

The dynamic mechanical behaviors of deep rocks are essentially influenced by complex geological occurrence conditions. However, the conventional SHPB system can only exert the axial dynamic loading on the rock specimen. The confining pressure cannot be directly applied to the rock specimen in the traditional SHPB system, limiting its extension to the measurement of dynamic responses of deep rocks. Therefore, the conventional SHPB system has been modified by scholars to evaluate the dynamic mechanical responses of rock-like materials under confining pressure.

2.1. SHPB with an active triaxial confinement device

SHPB system with a passive triaxial confinement device was initially extended to explore the dynamic behaviors of rocks under confinement. However, one of the critical issues of the passive triaxial confinement device is that the confinement cannot be exerted independently on the specimen, thus leading to the inconsistency of the confining pressure on the specimen during the dynamic loading process [34]. Therefore, an active confinement device has been proposed in SHPB system for investigating the dynamic mechanical properties of deep rocks [38].

The working principle of SHPB with the active triaxial confinement device is to encapsulate the specimen, parts of bars, and other components into the active triaxial confinement device, as shown in Fig. 2. An oil pump is utilized to exert the confining pressure to the specimen through the fluid medium (e.g., hydraulic oil, gas) in the confinement device. Taking the dynamic compression specimen as an example, when the specimen is subjected to lateral confining pressure, radial compressive deformation can be produced, leading to the mismatch between the end of the specimen and the end of the bar. As a result, the incident and transmitted bars could be detached from the specimen under lateral confining pressure, causing the failure of the dynamic experiment. Therefore, it is necessary to add an axial pressure device and a restraint device in SHPB system to restrain the movement of the bars, as shown in Fig. 2. Meanwhile, the axial pressure device can apply the axial pressure to the specimen, thus achieving the triaxial confining pressure on the specimens [39–42]. Furthermore, it is worth noting that some scholars have proposed using band clamps and brake bars to restrict the motion of the incident and transmitted bars, respectively [43]. In addition, four supporting rods between the front and rear plates are designed to provide the tension force for the confining pressure system. This can apply and maintain the triaxial confining pressure on the specimen during the dynamic loading process, thus improving the stability of the active triaxial confining pressure system and ensuring the

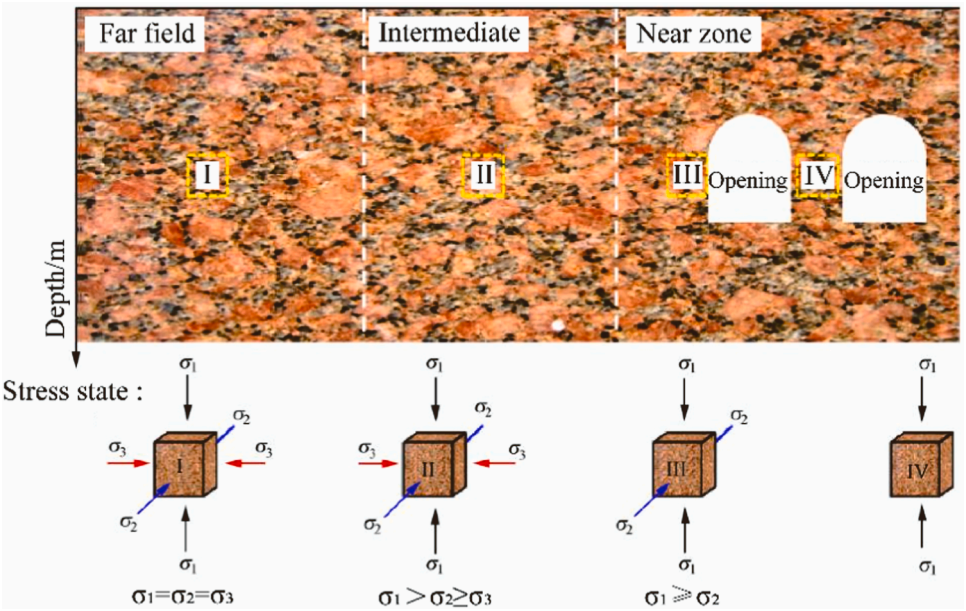

Fig. 1. In-situ stress states in deep underground excavation [14,15].

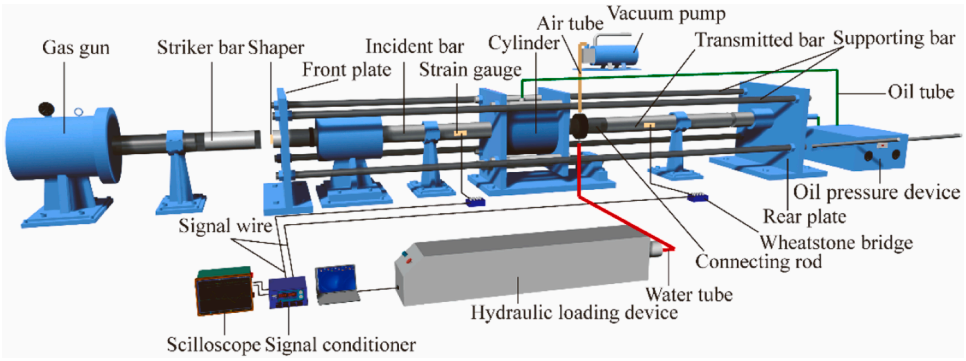

Fig. 2. Schematic of SHPB system with an active triaxial confinement device.

reliability of the experimental results. The schematic of SHPB with the active triaxial confinement system is shown in Fig. 2. According to the encapsulation types of the active triaxial confinement device, the sealing method can be further classified into lateral sealing and direct sealing.

To achieve active triaxial confinement on the specimen using lateral sealing, some scholars have proposed that the part of the bar near the specimen, the specimen, and other accessories are integrally sealed using rubber and two O-rings in the cylinder, as shown in Fig. 3(a). After that, the pressure generated by the oil (gas) injected into the cylinder can be indirectly applied to the side surface of the specimen through the rubber, thus completing the confining pressure [25,26,41,43,44]. The sleeve is designed to provide support for the bar without limiting the axial motion of the bars. Another design for achieving active triaxial confinement is to directly seal the part of the bar and the specimen with the rubber, removing the sleeve and the spacer (Fig. 3(b)) [34]. In this design, the oil (gas) pressure is still indirectly applied to the side surface of the specimen via the rubber. In the type I device, the rubber is fixed on the sleeve using the buckle, inducing friction between the bar/spacer and the rubber. In the type II device, the rubber is fixed directly on the surface of the bar so that the rubber moves with the bars during the dynamic loading process [34,41,43,45].

In the abovementioned sealing methods, due to the rubber between the specimen and the hydraulic oil, only dynamic compression experiments can be conducted using the cylindrical specimen whose diameter equals that of the bar. Therefore, a directly sealed device for active triaxial confinement was developed by abandoning the rubber, as shown in Fig. 3(c). To prevent the oil from penetrating the specimen, isolation technology is employed to pre-treat the specimen surface before the specimen is sandwiched between the bars. In such a case, this device can be used to perform dynamic compression [45], tension [46], and fracture [47] experiments with active triaxial confinement.

For the sealing methods mentioned above, the expansion and deformation of the specimen under the dynamic compressive loading result in the compression of the fluid in the cylinder, thus changing the confining pressure. Xia et al. [48] analyzed theoretically the change of the confining pressure during the dynamic loading and concluded that the increase in the cylinder volume can effectively reduce the pressure change of the hydraulic oil due to the specimen expansion. In addition,

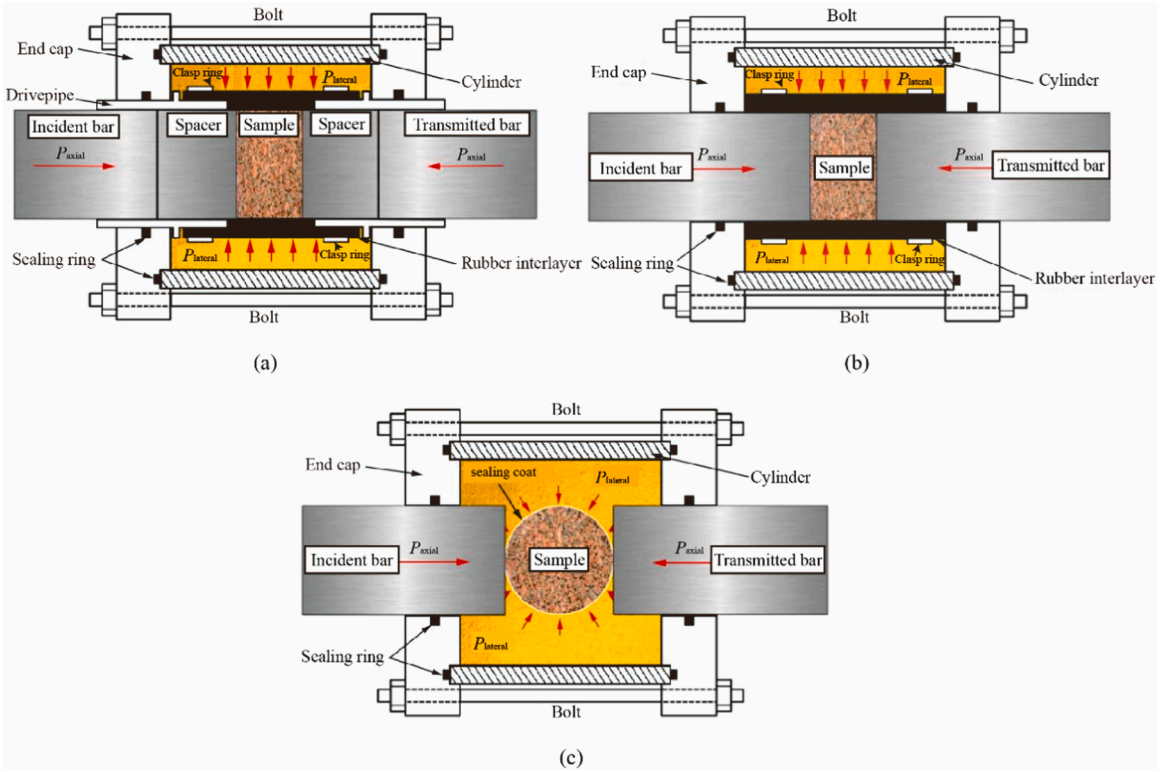

Fig. 3. (a) Type I lateral, (b) Type II lateral, and (c) directly sealed active confinement device.

because the dynamic pressurization can be dispersed when the specimen fails and the wave impedance between the specimen and the hydraulic oil is hugely different, the stress wave is essentially limited to the bars and the confining pressure remains basically constant. Furthermore, they provided the correction of the change of specimen dimensions caused by the triaxial confinement in the data processing to obtain the accurate dynamic stress-strain curves of the specimen under the confinement. Similarly, when the cylinder volume of the confinement device is relatively small, it is still necessary to consider the influence of the volume change of the hydraulic oil on the confinement. Moreover, Chen et al. [49] discussed in detail the complicated calculation of the stress balance in the specimen due to the axial preload in the bars and analyzed the effect of the separation between the front plate and the flange on the incidence bar on the wave propagation and the dynamic stress measurement.

2.2. Dynamic mechanical properties of rocks under confining pressures

Deep underground rocks are initially under in-situ stresses, and the stress state of deep rocks is changed after the excavation. According to the distance from the free face of the excavation, the in-situ stress state of rocks can be categorized into: (a) hydrostatic pressure zone in the far field, (b) triaxial stress zone in the middle field, and (c) pre-tensile stress zone in the near field [14]. When deep rocks are subjected to dynamic disturbances such as earthquake and operational blasting, the dynamic mechanical response of deep rocks is essentially important in underground rock engineering. Therefore, the dynamic compressive, tensile, shear, and fracture behaviors of deep rocks are discussed in this section.

2.2.1. Dynamic compressive behaviors of rocks under confining pressure

SHPB device with a confinement device can simulate the stress states

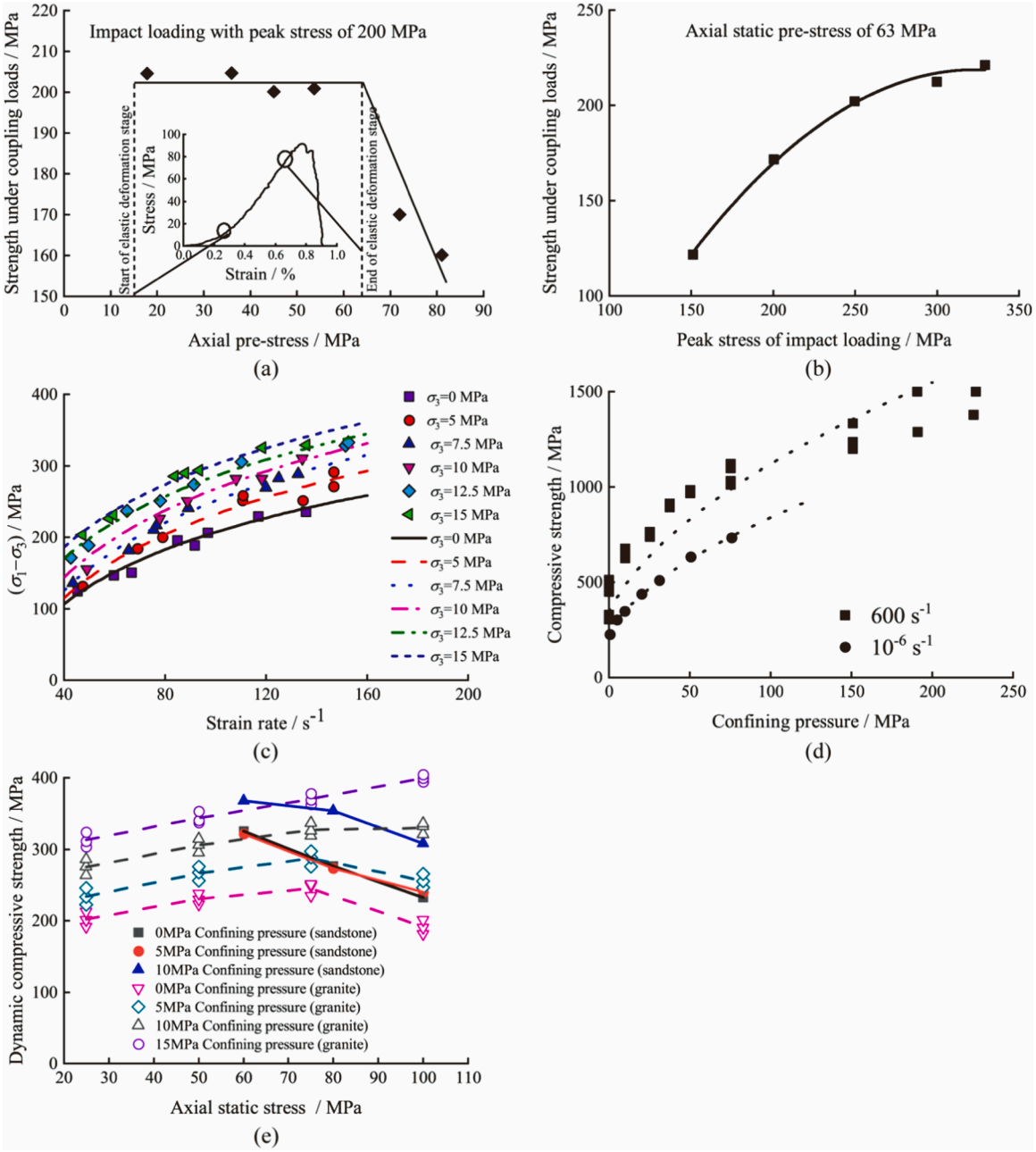

Fig. 4. Strengths of siltstone subjected to (a) the same impact loading but different axial pre-compression stresses [32] and (b) constant axial pre-compression stress of 63 MPa and different impact loads [32]; Dynamic compressive strengths of (c) sandstone under different stain rates and hydrostatic confinements [45], (d) Kuru granite subjected to hydrostatic confinement [58,59], and (e) sandstone and granite under different axial and lateral confinements [59,60].

of rocks in various fields mentioned above. According to the static stress state of specimens in dynamic compression experiments, Xia et al. [20] classified the static stress states into four types: (a) axial preload, (b) lateral confining pressure, (c) hydrostatic pressure, and (d) triaxial stress state. Since the confining pressure in the passive triaxial confinement device is not constant during the loading process [34], the dynamic rock experiments under the lateral confining pressure are currently conducted by using the active triaxial confinement device [32,38]. Because the pure lateral confining pressure cannot be exerted on the specimen without the axial stress, the dynamic mechanical properties of rocks under three types of stress states (axial preload, hydrostatic pressure, and triaxial stress state) are discussed in this subsection.

2.2.1.1. Dynamic compressive behaviors of rocks under axial preload. The procedure for analyzing the dynamic compressive strength of rocks under axial pressure is the same as that in the conventional dynamic compression experiments. Numerous experimental results indicate that the dynamic compressive strength of rocks under the axial preload demonstrates the rate dependence and the axial preload affects the dynamic compressive strength [50,51]. Under the same loading rate, the dynamic compressive strength of rocks first increases with the axial preload and then decreases if the axial preload continues increasing [52–54]. Also, the dynamic compressive strength of rocks generally reaches the peak value when the axial preload is about 60% of the static compressive strength of rocks [32,55]. For siltstones, the experimental results showed that when the axial preload is in the elastic deformation stage, the dynamic strength of siltstones is 40–60 MPa higher than the conventional dynamic compressive strength; When the axial pressure is greater than 80% of the static compressive strength, the compressive strength decreases rapidly; When the axial preload is more than 90% of the static compressive strength, the rock unstably fails (Fig. 4(a) [32]). When the axial preload is fixed, the dynamic compressive strength of siltstones first increases and then stabilizes with the increase in impact strength (Fig. 4(b) [32]). In general, the dynamic failure of rocks under the axial preload transferred from the tension-shear mixed mode to tensile mode as the increase in the impact velocity [55,56]. As the axial confinement increases, the failure mode of rocks transfers from a tension-dominated to a tension-shear mixed mode, and the level of fragmentation is positively correlated with the axial confinement [57].

2.2.1.2. Dynamic compressive behaviors of rocks under hydrostatic pressure. For various rocks (i.e., sandstone, granite, limestone, etc.), the experimental results showed that the dynamic compressive strength and the peak strain of rocks under hydrostatic pressures have an apparent strain rate dependence, and the dynamic compressive strength increases with the increase in the hydrostatic pressure at the same loading rate (e.g., Fig. 4(c)) [45,61,62]. In addition, as shown in Fig. 4(d), the experimental data indicated that, when the hydrostatic pressure is lower than 20 MPa, the dynamic compressive strength of granite increases at a higher rate with the hydrostatic pressure than that at the quasi-static loading condition, while the opposite is observed when the hydrostatic pressure is higher than 20 MPa [58]. Generally, the failure mode of rocks under hydrostatic pressures is gradually changed from tension to shear and the ductility of rocks significantly enhances with the increase in hydrostatic pressures [62,58,63,64].

2.2.1.3. Dynamic compressive behaviors of rocks under triaxial stress state. Recently, scholars have systematically studied the dynamic compressive mechanical properties of various rocks under different triaxial stress states [14,65], indicating that the dynamic compressive strength of rocks under triaxial stress states has an obvious rate dependence. The triaxial stress state is an essential factor affecting the dynamic compressive strength of rocks. As shown in Table 1, the dynamic compressive strength of rocks under triaxial stress states is closely related to the lithology and the loading conditions [59,66,67,60]. For example, the dynamic compressive strength of sandstone decreases with the increase of axial pressure at a certain lateral pressure [59]; however, the dynamic compressive strengths of red sandstone [66], dolomite [67], and granite [60] first increase and then decrease with the increase of axial pressure. Particularly, the dynamic compressive strength of granite is weakened with high axial pressure at low lateral pressures (< 10 MPa). When the lateral pressure is higher than 10 MPa, the dynamic compressive strength of granite increases with the increase of axial pressure (Fig. 4(e)) [59,60]. This phenomenon is mainly related to whether the rock specimen is in an elastic phase before being subjected to dynamic loading [68].

Table 1
Summary of previous studies on dynamic compression conditions of rock materials subjected to triaxial confinements [54,66,60,69–71].

Source	Types of rocks	Axial pressure/MPa	Lateral pressure/MPa	Strain rate/s^{-1}
Gong et al. [54]	Limestone	60/80/100 (52%/70%/96%)	0/5/10	105.93 ~ 114.35
Niu et al. [66,71]	Red sandstone	11/27/43 (20%/50%/80%)	0/5/10	50 ~ 350
Zhou et al. [69]	Dolomite	0/20/30 (0%/45%/67%)	0/5/10	62.5 ~ 103.6
Ma et al. [60]	Granite	25/50/75/100 (23%/45%/68%/91%)	0/5/10/15	90

2.2.2. Dynamic tensile and bending behaviors of rocks under confining pressure

Current experimental methods for measuring the tensile strength of rock-like materials are mainly classified into direct and indirect tension methods. Indirect tension methods primarily include the Brazilian Disc (BD) test, circular test, and bending test [72]. Due to the simplicity and ease of preparation, semi-disc specimens are often used with SHPB to study dynamic flexural tensile strength and its anisotropy in rocks [73–76].

Dynamic direct tensile experiments are mainly achieved by the Kolsky tensile bar system. Huang et al. [77] revealed that the dynamic direct tensile strength of Laurentian granite increases with the loading rate. Liu et al. [78] conducted dynamic direct tension experiments on rectangular granite specimens at different lateral pressures, showing that the dynamic direct tensile strength and the rate effect decrease when the lateral pressure increases. Although the direct tension test can directly obtain the true tensile strength of rocks, the indirect tensile method (i.e., the BD specimen) has been recommended by the International Society for Rock Mechanics and Rock Engineering (ISRM) to determine the dynamic tensile strength due to the complexity and limitations of the direct tensile test [51]. Therefore, dynamic tension experiments on rocks under the confining pressure are mainly conducted using the BD method.

The static loads applied to the BD specimen in the dynamic experiment can be classified into three categories: the axial load, the hydrostatic pressure, and the triaxial stress state. The loading rate is commonly used to describe the rate dependence of the dynamic tensile strength of rocks [51,75]. Chen et al. [79] reported that the dynamic BD tensile strength of marble deteriorates with the increase in the axial load. A similar phenomenon was observed for the granite specimen [80–82]. Ping et al. [81] investigated the effect of the axial load on the dynamic BD tensile strength and energy dissipation of limestone and found that the axial load enhances the reflected energy and decreases the energy absorbed by the BD specimen. In addition, Pei et al. [82] and Wu et al. [46] measured the total tensile strength (which is defined as the sum of the dynamic tensile strength and the static tensile stress induced by the preload) and the dynamic tensile strength of rocks under the preload by using the flattened and traditional BD method, indicating

that the total and dynamic tensile strengths of rocks exhibit significant rate-dependence, as shown in Fig. 5. Meanwhile, the dynamic tensile strength of granite specimens decreases with the preload (Fig. 5(a) [46]), but the total tensile strength of granite specimens is barely influenced by the preload (Fig. 5(b) [46]).

The device in Fig. 2 can also be used to complete the dynamic BD experiments for rocks under hydrostatic pressure. Wu et al. [14] theoretically proved the feasibility of dynamic BD experiments under hydrostatic pressure. The experimental results showed that the dynamic tensile strength of granite increases with the increase in the loading rate and the hydrostatic pressure; however, the rate effect gradually decreases with the increase of the hydrostatic pressure. The difference of microcracks in rocks under various hydrostatic pressures and loading rates can be successfully observed in CT images of the recovered specimens (in Fig. 6 [14]). Meanwhile, CT images provide further evidence of the aforementioned phenomenon that both loading rate and hydrostatic pressure affect the development of microcracks in the BD specimen.

If the axial load continues to increase and the confinement is constant, the triaxial stress state can be exerted on the BD specimen. A systematic study of the dynamic tension behaviors of rocks under the triaxial stress states has been performed using granite specimens [65]. Under triaxial stress states, the dynamic tensile strength of granite decreases with the increase of the axial load, and this trend is consistent with the dynamic tensile strength of granite under the pure axial load. However, the total tensile strength of granite is independent of the axial load. The mechanism of this phenomenon is consistent with that under the axial load. In addition, the dynamic failure pattern of BD specimens under triaxial stresses is consistent with that of the dynamic BD specimens without static stress, i.e., the tensile failure initiated from the center of the disc. Meanwhile, with the increase in loading rate, small wedge-shaped fragments are generated at the loading ends, which may be related to the secondary loading of the stress wave. With the increase of the axial load, fracture zones are easily formed in the center of the disc. This is caused by the existence of pre-damage in the rock under the axial load, which is prone to form multiple tensile failure paths under the impact [46,65,80].

In addition to the dynamic BD method, the dynamic semi-circular bending (SCB) experiment is an effective way to measure the dynamic flexible strength of rocks. Yao et al. [83] conducted dynamic SCB experiments on Laurentian granite (LG) under five axial loads and pointed out that the dynamic flexible strength of LG decreases with the axial load with an evident rate dependence (Fig. 7(a)). It is noteworthy that the total flexible strength of LG (which is defined as the sum of the dynamic flexible strength and the static flexible stress induced by the axial load) is generally independent of the axial load (Fig. 7(b)). In addition, the total flexible strength of rocks under the axial load is slightly higher than the total BD tensile strength, and this discrepancy also exists in the flexible and tensile strength of rocks under static and dynamic loading conditions without confining pressure [72,84–87]. This difference is mainly attributed to the anisotropy and heterogeneity of rocks [88]. Furthermore, Xia et al. [72,83,85,89] proposed a non-localized damage model to reconcile the discrepancy between the BD tensile strength and the flexible strength and found that the corrected dynamic flexible strength is consistent with the dynamic BD tensile strength at different axial loads (Fig. 8 [83]).

2.2.3. *Dynamic shear behaviors of rocks under confining pressure*

As early as the 1970 s, Lipkin et al. [90,91] conducted dynamic pure shear experiments using short thin-walled tubular specimens with the split Hopkinson torsional bar (SHTB). However, it is difficult to extensively adopt this tubular specimen to measure the dynamic shear behaviors of materials due to the complexity of the preparation of tubular specimens and SHTB accessories. Therefore, some scholars have proposed other methods to measure the shear strength of materials, such as a compression-shear method [92], a direct shear method [93], a punch shear method [94], and a triaxial compression method [95,96]. Among these methods abovementioned, some scholars combined the punch shear method with the conventional SHPB system to measure the dynamic shear strength of materials due to the easy specimen preparation, simple operation, and high repeatability of the punch shear method [37]. Huang et al. [94] conducted the dynamic punch shear experiment in SHPB system and verified the feasibility of this method for measuring the dynamic shear strength of rocks. In 2018, the dynamic punch shear method was recommended as the group standard for determining the dynamic shear strength of rocks in the China Society of Explosive and Blasting [97]. Xu et al. [37] proposed a dynamic punch shear method for rocks under confinement using a Hoek cell and performed the dynamic punch shear experiment on green sandstone under three confining pressures (0, 10, and 20 MPa). The experimental results showed that the dynamic shear strength of sandstone under the confinement increases with the loading rate and the confinement, and further demonstrated that the dynamic internal friction angle of the sandstone was nearly independent of the loading rate (Fig. 9 [37]). In addition, Xu and Dai [98] conducted compressive shear impact tests on the cylindrical specimen with an inclined cross-section using SHPB system with a static preload device. The rate-dependence of the dynamic shear strength of green sandstone was observed.

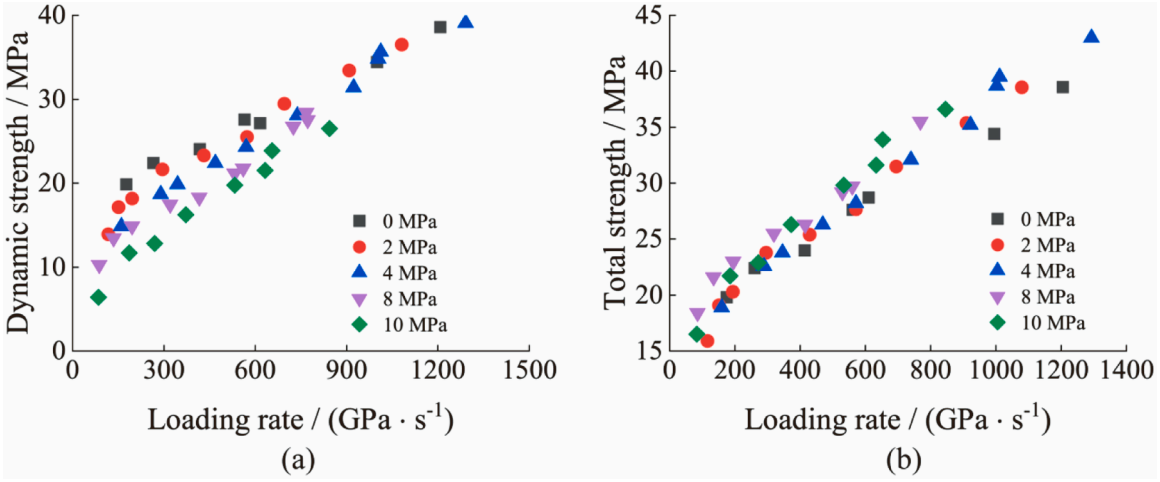

Fig. 5. (a) Dynamic and (b) total tensile strength versus loading rate for different preloads [46].

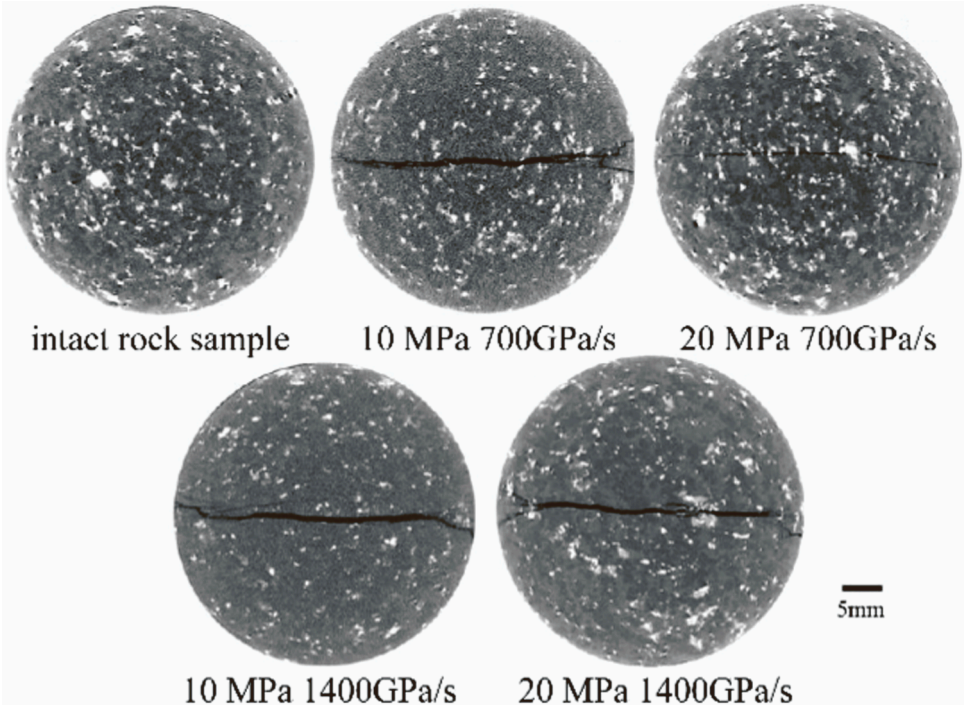

Fig. 6. Micro-CT images of recovered specimens under different loading rates and hydrostatic pressures [14].

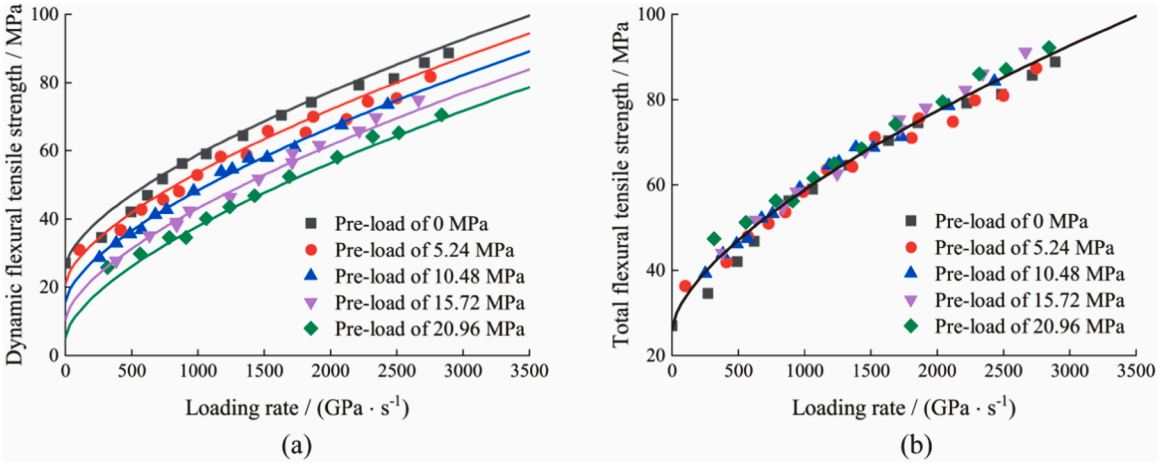

Fig. 7. (a) Dynamic and (b) total flexural tensile strengths of granite versus loading rate for different preloads [83].

2.3. *Dynamic fracture behaviors of rocks under confinement*

2.3.1. *Dynamic mode-I fracture behaviors of rocks under confinement*

The mode-I fracture failure of rocks is common in nature and a variety of experimental methods have been proposed by scholars to determine the mode-I fracture behaviors of rocks, including wedge loaded tension method (WLCT) [99], single slotted bending method (SENB) [100], straight slotted Brazilian disc method (CSTBD) [101], chevron slotted Brazilian disc method (CCNBD) [102–106], chevron slotted semi-circular disc method (CCNSBD) [107], short bar method (SR) [108–110], three-point chevron bending (CB), and straight slotted semi-circular disc method (NSCB) [51]. Among these methods, the NSCB method has been recommended by ISRM for determining the dynamic mode-I fracture toughness of rocks since 2012 due to its various advantages: the easy specimen preparation, the simple assembly, and the convenient achievement of the force balance in the specimen during the dynamic loading [111]. In 2014, the NSCB method was also recommended by ISRM for determining the static mode-I fracture toughness of rocks [112]. Therefore, the NSCB specimen under different confining pressures is mainly discussed in this section.

The dynamic mode-I fracture toughness of rocks under the axial load was measured by Chen et al. [113] using SHPB system with an active triaxial confinement device (Fig. 2). As shown in Fig. 10(a), the results show that the dynamic fracture toughness of Heshuo granite under a certain axial load is significantly rate dependent and decreases with the increase of the axial load at a specific loading rate (Fig. 10(a)), indicating that the axial load causes the pre-tension stress at the crack tip and further reduces the dynamic impact resistance of rocks. Consequently, the crack in the NSCB specimen under the axial load can be expanded under the low impact velocity. Moreover, the total mode-I fracture toughness of granite, which is defined as the sum of dynamic fracture toughness and static stress intensity factor induced by the axial load, was measured at various loading rates, as shown in Fig. 10(b). It shows that the total fracture toughness increases with the increase of the

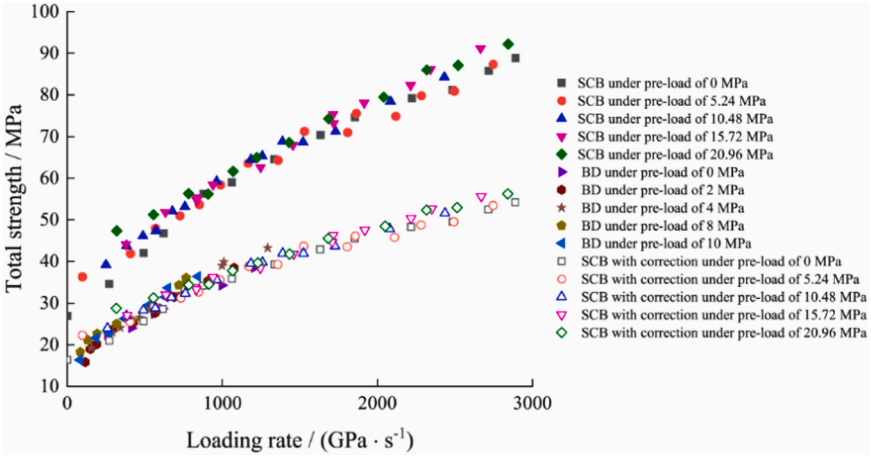

Fig. 8. Comparison of strengths from dynamic SCB and BD tests with preload as well as reconciliation by nonlocal failure model [83].

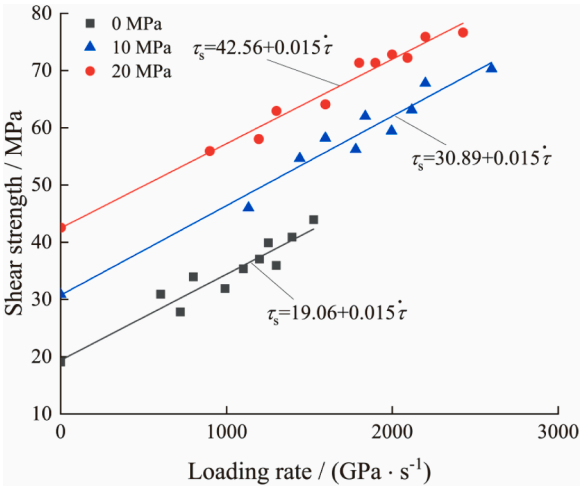

Fig. 9. Dynamic punch shear strengths under different loading rates and confining pressures [37].

axial pressure at a certain loading rate. Furthermore, Yao et al. [47] conducted a dynamic NSCB experiment using SHPB system with an active triaxial confinement device in Figs. 2 and 3(c) and measured the dynamic mode-I fracture toughness of Laurentian granite under five hydrostatic pressures (0, 5, 10, 15, and 20 MPa). As shown in Fig. 11, the dynamic mode-I fracture toughness of granite increases with the increase of the hydrostatic pressure, which is attributed to the fact that the damage region of the NSCB specimen along the fracture path decreases with the hydrostatic pressure. At high hydrostatic pressure, more microcracks are closed, leading to a decrease in the damage zone.

2.3.2. *Dynamic mode-II fracture behaviors of rocks under confinement*

Several testing methods have been proposed for determining the mode-II fracture or mixed mode I/II fracture behaviors of rocks: (a) Fracture deviates from the notch or shear direction: single (or double) notched antisymmetric four-point bending method for pure shear fracture [114–117], Arcan specimen with notch [118,119], Cracked straight-through Brazilian disc (CSTBD) [120–122], Semi-circular bend with inclined notch [123–125]; (b) Fracture aligns with notch or shear direction: shear box test; punch through shear (PTS), short beam in compression (SBC), and short core in compression (SCC). To obtain the mode-II fracture toughness (K_{IIC}) under the pure shear stress, Rao et al. [126] proposed a shear box test with two symmetrically notched (or single center notch) rectangular specimens. The PTS method with cylindrical and rectangular specimens was initially developed to investigate the effect of pressure on mode-II fracture toughness [127–130]. Because of the advantages of cylindrical specimens in preparation and assembly, the PTS method with the cylindrical specimen has been suggested by ISRM for determining static mode-II fracture toughness of rocks since 2015 [131]. To further simplify the specimen preparation

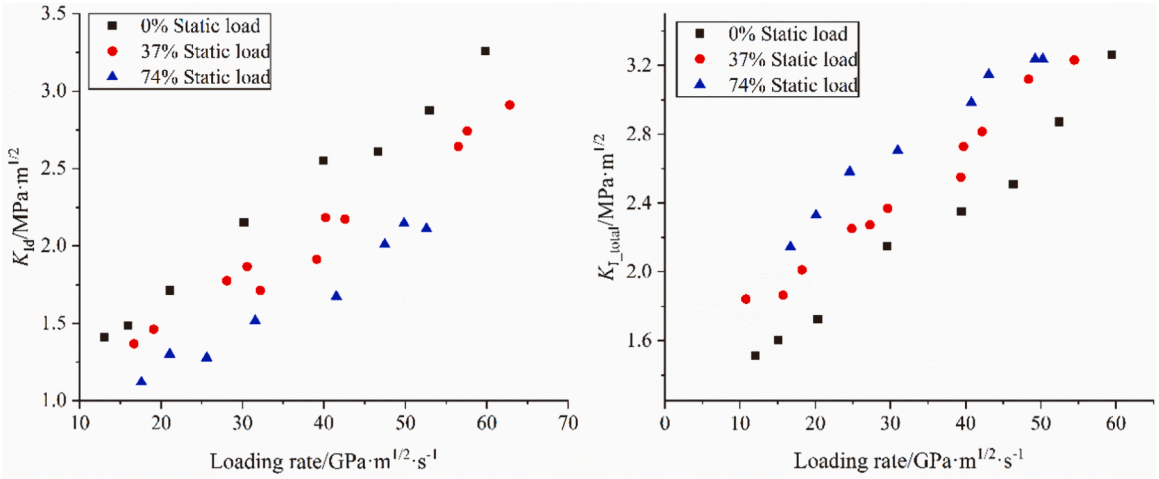

Fig. 10. Relation between mode-I fracture toughness and loading rate of rocks under different preloads [113].

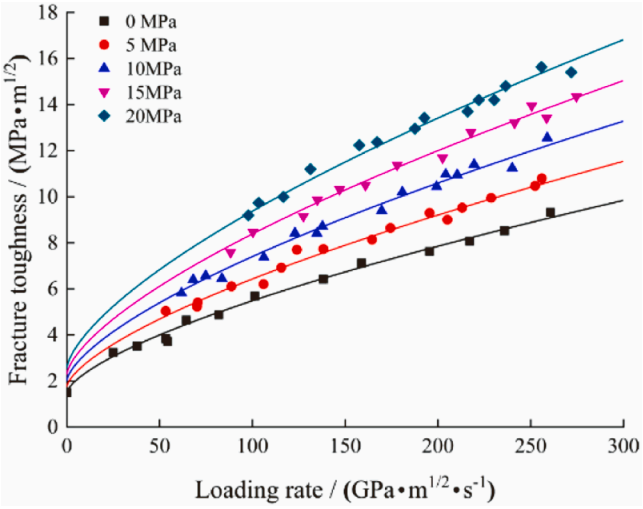

Fig. 11. Dynamic fracture toughness versus loading rate for different hydrostatic pressures [47].

and experiment procedure, the SBC [132] and the SCC [133,134] have been proposed for measuring static mode-II fracture toughness of concretes and other rock-like materials. To measure the dynamic mode-II fracture toughness of rocks, Yao et al. [135] designed the dynamic PTS method with the cylindrical specimen on SHPB (Fig. 12) and proved the feasibility of this method by satisfying the force balance between the two loading ends of the specimen during the dynamic loading period. The rate dependence of the dynamic mode-II fracture toughness of Fangshan marble was observed. Further, Yao et al. [36] proposed the dynamic PTS method with confinement (Fig. 12) to measure the dynamic mode-II fracture toughness of rocks under the confining pressure. The experimental results show that the dynamic K_{IIC} increases with the increase of the confining pressure at a certain loading rate, as shown in Fig. 13(a) [36]. The fracture pattern inside the recovered PTS specimens (Fig. 13(b) [36]) indicates that the shear fracture is dominant under each confining pressure condition, validating the feasibility of this method to measure the mode-II fracture toughness of rocks under the confining pressure. It was also observed that with the increase of the confining pressure, the wing crack disappears, and the ring crack is formed gradually. Moreover, Yao et al. [136] designed the SCC method using SHPB system with an active triaxial confinement device (Fig. 2) to measure the dynamic K_{IIC} of rocks subjected to different hydrostatic pressures. The experimental results indicate that the failure mode of the rock SCC specimen under hydrostatic pressure is the shear fracture and the dynamic rock K_{IIC} is barely affected by hydrostatic pressures at a given loading rate (Fig. 14(a)). However, the dynamic fracture energy of rocks is enhanced with loading rates and hydrostatic pressures (Fig. 14

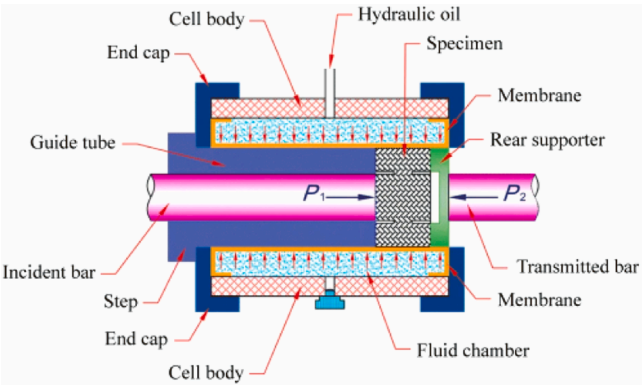

Fig. 12. Dynamic PTS experiment with confining pressure [36].

(b)). Recently, the applicability of the PTS method and the SCC method to determine the dynamic K_{IIC} of rocks under preload and confining pressure was verified by Yao et al. [137]. As shown in Fig. 14(c), the dynamic K_{IIC} of rocks decreases with the preload. The total K_{IIC} of rocks derived from the PTS/SCC specimens are almost consistent under the same loading rate regardless of the magnitude of the preload exerted on the PTS/SCC specimens (Fig. 14(d)). In addition, the dynamic K_{IIC} of rocks under confining pressures derived from the PTS method is remarkably different from that obtained from the SCC method, and theoretical analysis was conducted to quantitatively rationalize this discrepancy using the difference of the normal stress state and the stress intensity factor in these two methods (Fig. 14(e)). The exploration of the determination of dynamic mode-II fracture of rocks under confining pressures is still preliminary, and the effective experimental methods need to be further explored.

3. True triaxial SHPB system

In real deep underground rock engineering, rocks are naturally subjected to true triaxial in-situ stresses, in which the second and third principal stresses are different. Consequently, the dynamic mechanical responses of rocks under the true triaxial stress are quite distinct from those under the triaxial confinement, and Some scholars have modified the conventional SHPB to suit studying the dynamic mechanical responses of rocks under the true triaxial stress.

3.1. SHPB with a true triaxial loading device

Based on the concept of the static true triaxial loading device, some researchers have proposed an SHPB system with true triaxial loading. The concept of the true triaxial SHPB system was initially proposed by Zhao, Cadoni, and Albertini in 2009 [15]. Currently, the true triaxial SHPB system has been further developed [15,138,139]. Xu et al. [138–140] assess the dynamic compressive behaviors of concrete under the static true triaxial stress conditions using the true triaxial SHPB system. They discussed the core issues of the true triaxial SHPB system, including the dynamic stress-strain relationship of rocks under the true triaxial stress state and the influence of the intermediate principal stress on the dynamic strength of rocks under the true triaxial stress state. Liu et al. [15] used the true triaxial SHPB system to obtain the dynamic compressive behaviors of sandstone under the true triaxial stress state and theoretically analyzed the dynamic stress and strain of the specimens at various strain rates, contributing to the development of the true triaxial SHPB.

As shown in Fig. 15(a), during the testing process using the true triaxial SHPB system, a cubic specimen is placed in the center of six square bars, The specimen is under the true static triaxial stress through the square bars using the hydraulic system. After that, a stress wave is generated from the free end of the incident square bar. Upon reaching the specimen, the stress wave is reflected and transmitted at the ends of the bar/specimen interface, and the reflected wave propagates back into the incident bar. Meanwhile, the transmitted stress waves continue to propagate through five transmitted bars. Based on the stress wave theory, the stress-strain relationship in the three directions of the specimen can be obtained.

In addition, as shown in Fig. 15(b), Xie et al. [142] developed a novel true triaxial electromagnetic Hopkinson bar (TEHB) system, which provides a cutting-edge testing platform for studying the three-dimensional (3D) rock dynamic behavior subjected to the coupled triaxial dynamic impacts, under both triaxial in situ stress and strain rates of $10^1 \sim 10^3\ s^{-1}$. The superiorities of the TEHB over the conventional dynamic testing apparatuses mainly include: (1) the controllable and adjustable generation of stress pulse; (2) the synchronous, repeatable, and precise generation of multiple identical stress pulses; (3) the convenient and precise achievement of the stress equilibrium of the specimen; (4) the easy replicability of the coupled triaxial dynamic

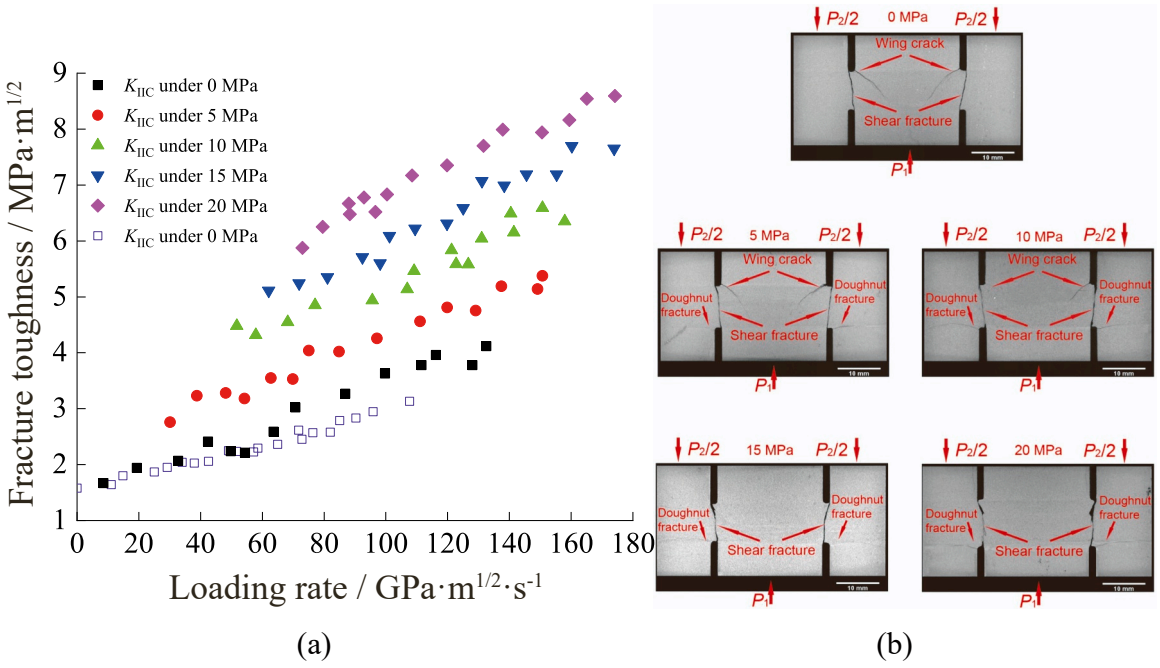

Fig. 13. (a) Dynamic mode-II fracture toughness and (b) fracture pattern of PTS specimens under various confining pressures [36].

impact and triaxial in situ stress conditions. The TEHB can achieve the compression, tension, and fracture tests by imposing multi-directional dynamic impact on the cubic rock specimen under in situ stress conditions.

3.2. Dynamic behaviors of rocks under true triaxial stress state

Scholars have conducted dynamic experiments using the true triaxial SHPB system to explore the dynamic behaviors of rocks under a true triaxial stress state. Zhang et al. [15] systematically studied the dynamic responses of sandstone under uniaxial, biaxial, and triaxial compression using the true triaxial SHPB system. Dynamic stress-strain curves share a linear region at the beginning of dynamic loading, and the peak strain shows a decreasing trend as the confining stresses increase. Moreover, the elastic modulus increases with confinement conditions varying from uniaxial, and biaxial to triaxial compression. As shown in Fig. 16, the dynamic strength of rocks is also dependent on confinements, and it decreases with the increasing axial pre-stress σ_1 along impact direction but enhances with the increase of lateral pre-stresses σ_2 and σ_3, which may be caused by both the lateral confinement on the specimen and the dynamic friction of the contact surfaces between the specimen and lateral bars. Microcracks inside specimens are reactivated by pre-stress σ_1, and thus a damaged state is induced. However, the dilatancy for crack growth in the σ_1 direction is suppressed by the lateral confining pre-stresses. Failure modes of sandstone also exhibit confinement dependence at the same impact velocity. Rocks can be pulverized into powder in uniaxial compression, and the rock ejection phenomenon occurs from the free surface in dynamic biaxial compression. However, in dynamic triaxial compression, rocks are fractured with a macroscopic shear fracture at low pre-stress states and remain intact in shape with great damage when pre-stress increases.

Chen et al. [143] studied the effect of the strain rate and intermediate principal stress on the dynamic behaviors of concretes by using the true triaxial SHPB system. Under static biaxial confinements, the dynamic shear strength τ_d decreases with the increase of σ_d=1/2($\sigma_1 + \sigma_3$), and the experimental data deviate greatly from the dynamic Mohr-Coulomb strength (Fig. 17(a)), which indicates evidence of the effect of intermediate principal stress. Under triaxial confinements, the shear strength τ_d increases with the increase of σ_d, and the experimental data show good consistency with the dynamic Mohr-Coulomb strength (Fig. 17(b)), and the effect of intermediate principal stress seems to be not evident. The Drucker-Prager (D-P) model was then modified to describe the intermediate principal stress dependence and loading rate effect by introducing the Lode angle (θ) and the strain rate.

4. Coupled hydraulic-mechanical experimental system for deep rocks

The high pore pressure and differential pore pressure are the basic attributes of deep rock engineering, and the artificial or natural dynamic disturbances may increase the possibility of deep geological disasters (e.g., earthquake and rockburst). Therefore, the dynamic mechanical properties of rocks under deep geological hydraulic-mechanical coupling conditions, which are essential for revealing the dynamic failure mechanism of deep rocks, have attracted great attention worldwide in recent years [9]. However, the research progress on the dynamic mechanical response of deep rocks subjected to high pore pressure and differential pore pressure is rather tardy due to the limitation of the experimental instrument. Recently, an experimental system has been developed by researchers to systematically explore the influence of the differential pore pressure or high pore pressure on the dynamic failure mechanism and permeability evolution of deep rocks under in-situ stresses.

4.1. SHPB with a coupled hydraulic-mechanical device

To study the dynamic mechanical response of deep rocks subjected to high pore pressure and confining pressure, a novel dynamic in-situ seepage experimental system and method for rocks based on the SHPB system has recently been developed by Xu et al. [144], which provides a cutting-edge testing platform for investigating the dynamic mechanical properties of deep rocks under various pore pressure and confinement conditions. Zou et al. [145] conducted a series of compression tests to investigate the thermal-hydraulic-mechanical behaviors of sandstone. However, details of the experimental design were missing. Recently, based on the active triaxial confinement device (Fig. 2), Zhao et al. [146] developed a novel triaxial SHPB system with a pore pressure loading cell for quantifying the dynamic compressive response of rocks subjected to

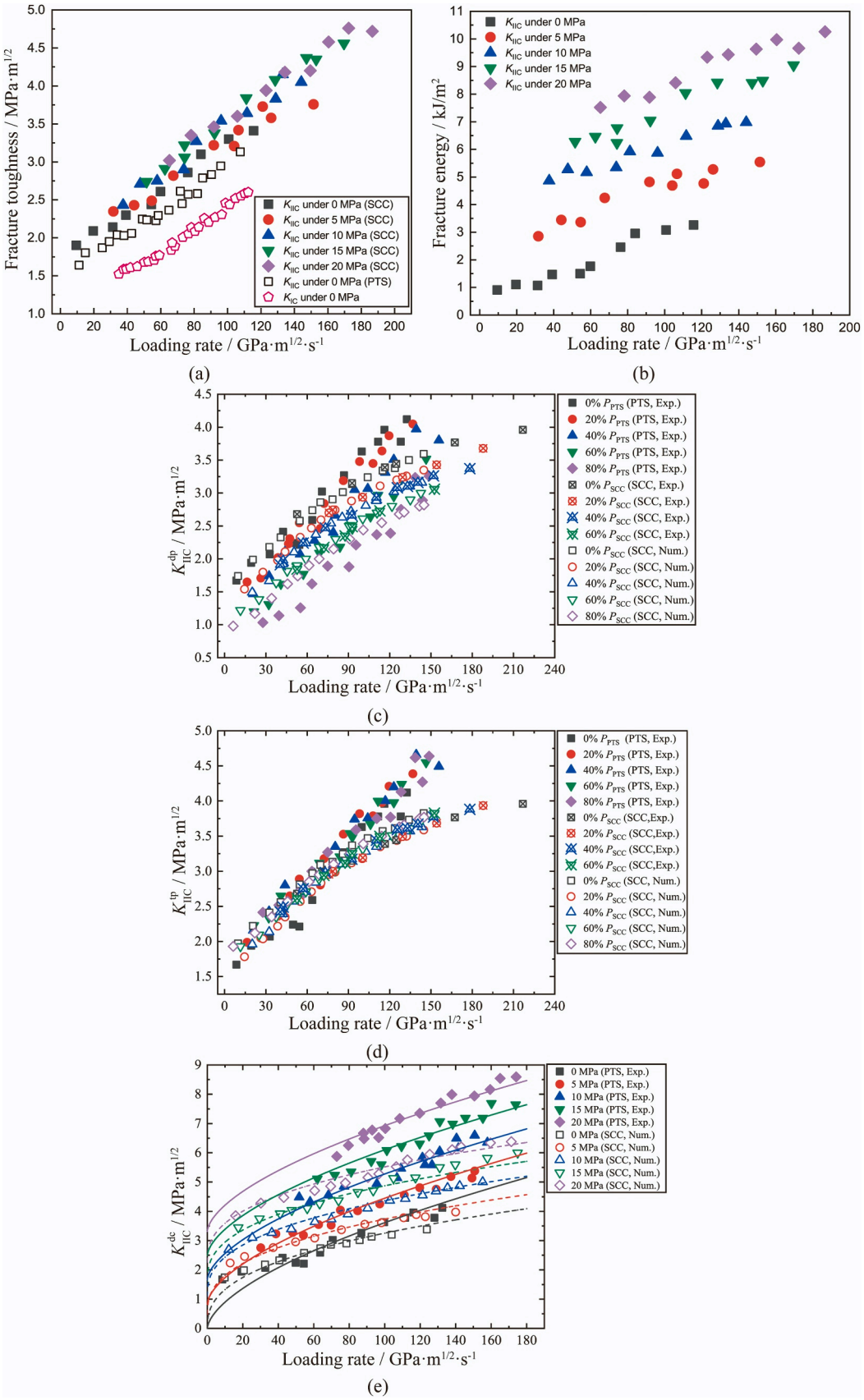

Fig. 14. (a) Fracture toughness and (b) fracture energy of FM SCC specimen with different hydrostatic pressures; (c) Dynamic and (d) total fracture toughness of FM obtained from PTS and SCC specimens with various preloads; (e) Dynamic fracture toughness obtained from PTS and SCC specimens with various confining pressures.

Fig. 15. (a) Photo of the triaxial Hopkinson bar system [15] and (b) the schematic of the TEHB system [141].

triaxial stress and pore pressure. The novel triaxial SHPB experimental system with a pore pressure loading cell was introduced in detail by Zhao et al. [146]. Later, Chen et al. [147] modified the pore pressure loading cell and developed a coupled hydraulic-mechanical device in the triaxial SHPB system, as shown in Fig. 18. In this way, the dynamic compressive behaviors of rocks subjected to triaxial stress and differential pore pressure were quantified.

Specifically, as illustrated in Fig. 18, this system is mainly composed of a conventional SHPB system, an in-situ stress system, a differential pore pressure system, and a data acquisition system. The conventional SHPB system and the in-situ stress device are identical to SHPB with an active triaxial confinement device in Fig. 2. The schematic of the differential pore pressure device is shown in Fig. 18. Since the differential pore pressure can only be exerted on rocks under the in-situ stress environment, the differential pore pressure device was designed to assemble into the triaxial confinement SHPB system. The differential pore pressure system consists of an electro-hydraulic servo loading device, a guide bar, and a modified incident bar with two symmetrical pinholes and a circular diversion groove, two sealing flanges, a vacuum pump, metal water pipes, and valves. The modified incident and guide bars are essential for differential pore pressure loading and stress wave transmission. Thus, the structures of the incident bar and the guide bar are specially designed. The guide bar, made of the same material as the bars, passes through the confining cylinder. At the ends of the modified incident bar and the guide bar, diversion grooves in the shape of a circle and cross are made, aiming to uniformly disperse the water pressure on two ends of the rock specimen. One pinhole in the guide bar is utilized for vacuuming the air and the other is used as the fluid transport channel. With the design of two pinholes in the guide bar, the air can be quickly discharged to ensure that the servo water pressure loading device is filled with water. If there is no pinhole in the incident bar, the high pore pressure can be effectively exerted on the rock specimen under the triaxial confinement. If the water is allowed to permeate through the rock specimen, two small pinholes are drilled along the axis of the incident bar and diversion grooves are manufactured on the end of the incident bar. Similar to the guide bar, the diversion grooves are in contact with the ambient atmosphere through two pinholes. These two pinholes in the incident bar are used as the drainage channels, with which the water permeated through the rock specimen discharges to the air and the water pressure on this end of the rock specimen equals the atmospheric pressure. The electrohydraulic servo water pressure loading device is controlled by a computer and can perform servo control in multiple modes, e.g., a constant water pressure mode and a constant flow rate mode. Several real-time parameters (including the water pressure, the displacement of the hydraulic press lever, and the flow rate) can be recorded by the water pressure data acquisition system through the water pressure sensor and LVDT (Linear Variable Differential Transformer). The water pressure data can be collected by a computer that also controls the water pressure machine.

4.2. *Dynamic behaviors of rocks subjected to coupled hydraulic-mechanical loading condition*

Currently, most existing studies focused on the impact dynamic response of rocks under the coupling of high temperature and water or a single state of different water content. Few attempts have yet been made to investigate the dynamic mechanical and transport behaviors of deep rocks under coupled hydraulic-mechanical loading conditions. Hence, we discussed the results on the dynamic behaviors of rocks under both differential pore pressure and triaxial stress state in this section.

Li et al. [148] and Zhou et al. [149] developed a fracture-damage model to estimate the stress intensity factor of the pre-determined crack tip of rocks under a compressive shear stress field and a seepage field. The water pressure was introduced to the prefabricated single crack through a water injection hole inside the rock specimen and then dynamic impact tests were conducted on these pre-cracked specimens using SHPB. Experimental results verified that the initial crack strength increases with the confining pressure and decreases with the seepage water pressure (Fig. 19(a) and (b)). The seepage water pressure is exacerbated in the crack extension. The dynamic load consistent with the direction of maximum principal stress increases the mode-I stress intensity factor, and the crack initiation angle changes with the dynamic load. Wang et al. [150] developed an experimental device that can provide both differential pore pressure and confining pressure on the specimen based on SHPB system, showing that the external water pressure increases the dynamic cohesion between the particles and subsequently increases the dynamic fracture toughness of coal (Fig. 19 (c)).

Zhao et al. [146] used the true triaxial SHPB system to determine the dynamic strength of rocks subjected to coupled hydraulic-mechanical loading. The results indicate that the dynamic compressive strength of rocks increases with the loading rate and the confining pressure but decreases with the pore pressure. In addition, single shear failure and X-type conjugate shear failure are the most common dynamic failure modes under hydrostatic confinement and pore pressure conditions (Fig. 20). It also found that the cohesion in the Mohr-Coulomb failure criterion has a strong dependence on the loading rate but is independent of the pore pressure and confining pressure. The free water has a bidirectional effect on the dynamic strength, i.e., the water-wedge effect facilitates the crack propagation and then reduces the rock strength, while the Stefan effect impedes the damage of the pore structure and has an enhancing effect on the dynamic strength. The experimental results prove that the true triaxial SHPB system is reliable and flexible for quantifying the dynamic compressive response of deep rocks considering the confinement and the pore pressure.

Chen et al. [147] utilized the true triaxial SHPB system to evaluate

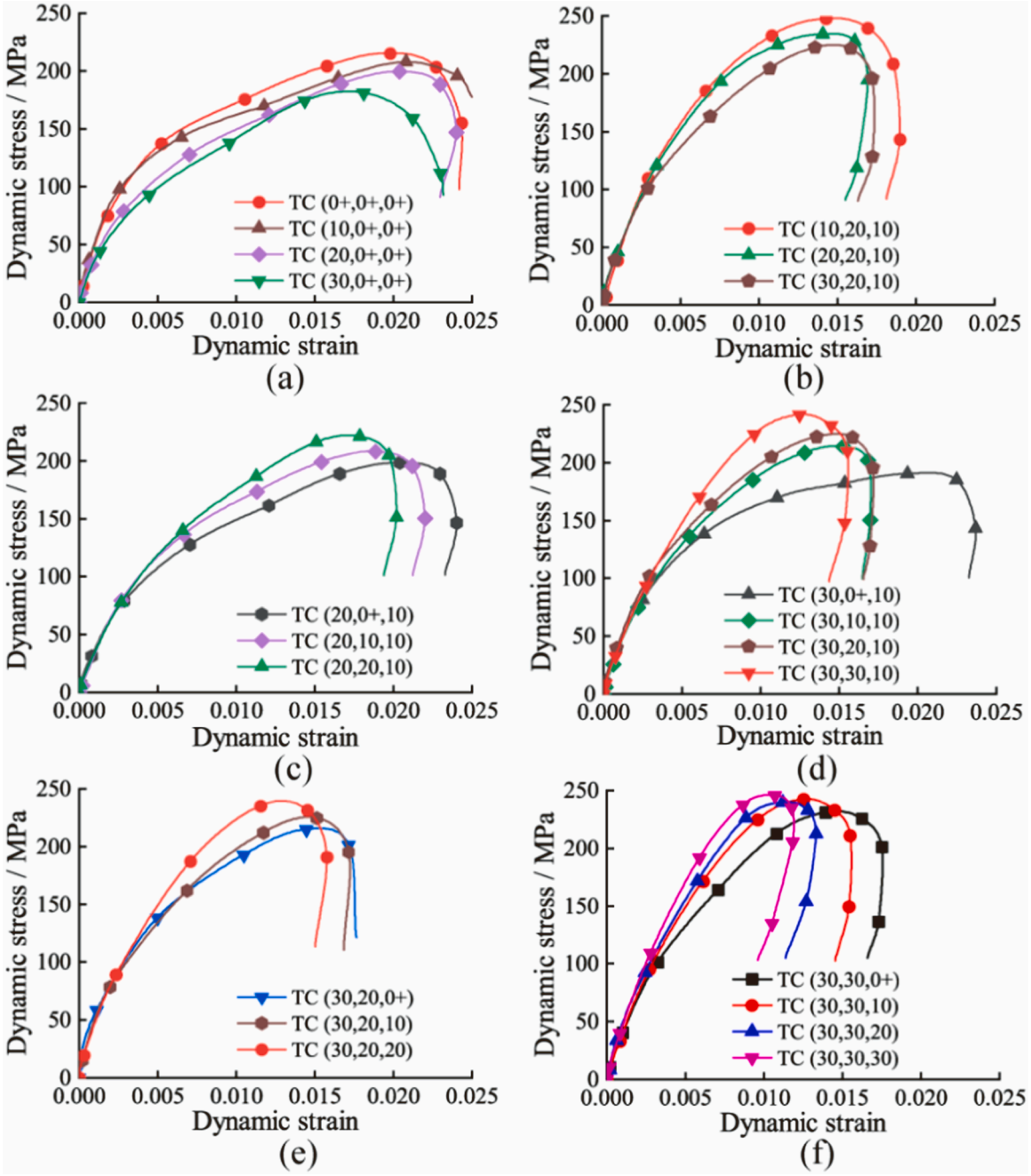

Fig. 16. Dynamic stress-strain curves of sandstone at the impact velocity of 20 m/s under triaxial compression: (a) and (b) effects of σ_1; (c) and (d) effects of σ_2; (e) and (f) effects of σ_3 [15].

the effect of differential pore pressure on the dynamic mechanical properties and permeability evolution of rocks under different differential pore pressures, different confining pressures, and different strain rates. The stress-strain curves change with the increase of impact number, and the cyclic impacts with the constant incident energy deteriorate the dynamic compressive strength of GS (Fig. 21 (a) and (b)). The permeability of GS first increases and then decreases with the impact number (Fig. 22(a)). The differential pore pressure enhanced the permeability of GS under the same impact cycle (Fig. 22(b)). The main fracture mode of the GS specimen is mainly compressive-shear fracture in combination with a tensile fracture in the middle of the specimen due to the coupling effect of the reflected stress wave and the hydraulic-confining pressure. These studies mentioned above also indicate that the (differential) pore pressure alters the effective stress acting on the rock skeleton to affect the dynamic compressive behaviors and transport properties of rocks and further induce geological disasters [9].

5. Conclusions

Understanding the dynamic responses of deep rocks is of great significance in the improvement of the safety and efficiency of deep rock engineering. This paper focuses on advances in dynamic tests of deep rocks considering in-situ mechanical and hydraulic conditions, reviewing the new SHPB experimental devices and technologies and their applications in measuring the dynamic responses of deep rocks in the laboratory. Furthermore, this paper summarizes the results of the dynamic test of deep rock under different in-situ mechanical and hydraulic

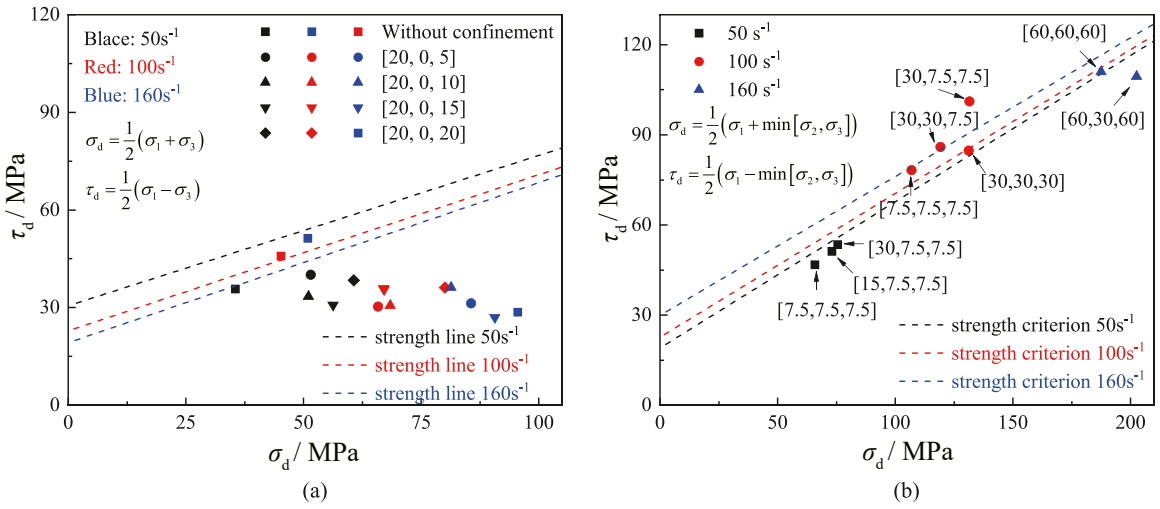

Fig. 17. The shear strength vs. σ_d of concretes (a) under static biaxial confinement and (b) under triaxial static confinement [143].

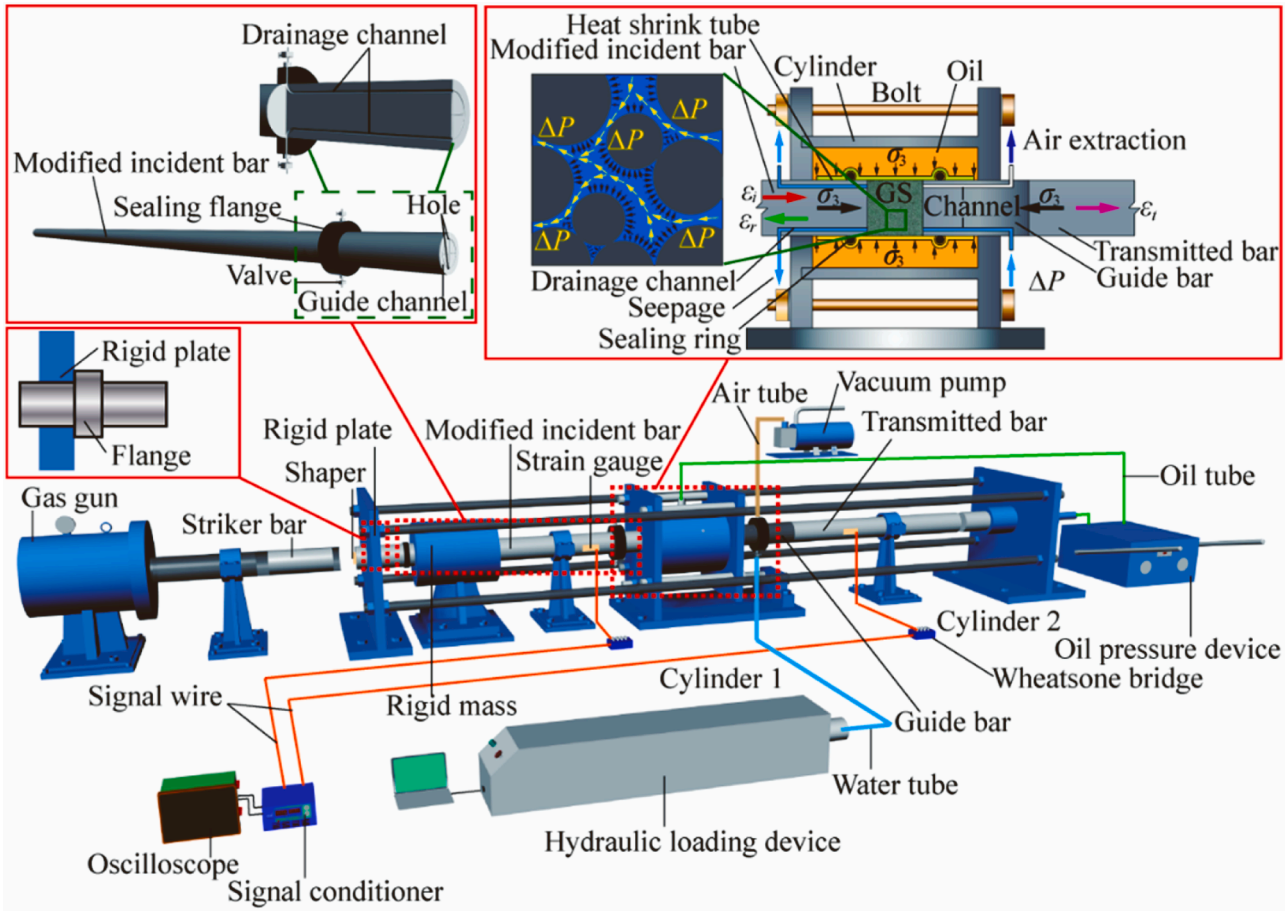

Fig. 18. The triaxial SHPB system with the differential pore pressure system [146].

conditions. The main conclusions are drawn as follows:

The triaxial confinement SHPB system has become a prevailing apparatus in the field of deep rock dynamics. The principles of the triaxial confinement SHPB system are introduced and discussed. the passive triaxial confinement SHPB device and true triaxial SHPB device cannot guarantee a constant confining pressure during the dynamic loading. Among the active triaxial confinement SHPB devices, the directly sealed active confinement method is widely adaptable and reliable because the bar ends can be sealed directly into the cylinder with the specimen, and multiple dynamic mechanical properties of rocks can be measured at different confining pressures.

The dynamic compressive strength and failure mode of rocks are obviously affected by the confining pressure. The dynamic compressive strength of rocks generally increases with the confining pressure and has a significant rate dependence under the same confining pressure. When the axial preload is lower than a certain value, the dynamic compressive strength of rocks is enhanced; however, when the axial preload exceeds a specific value, the dynamic compressive strength of rocks deteriorates

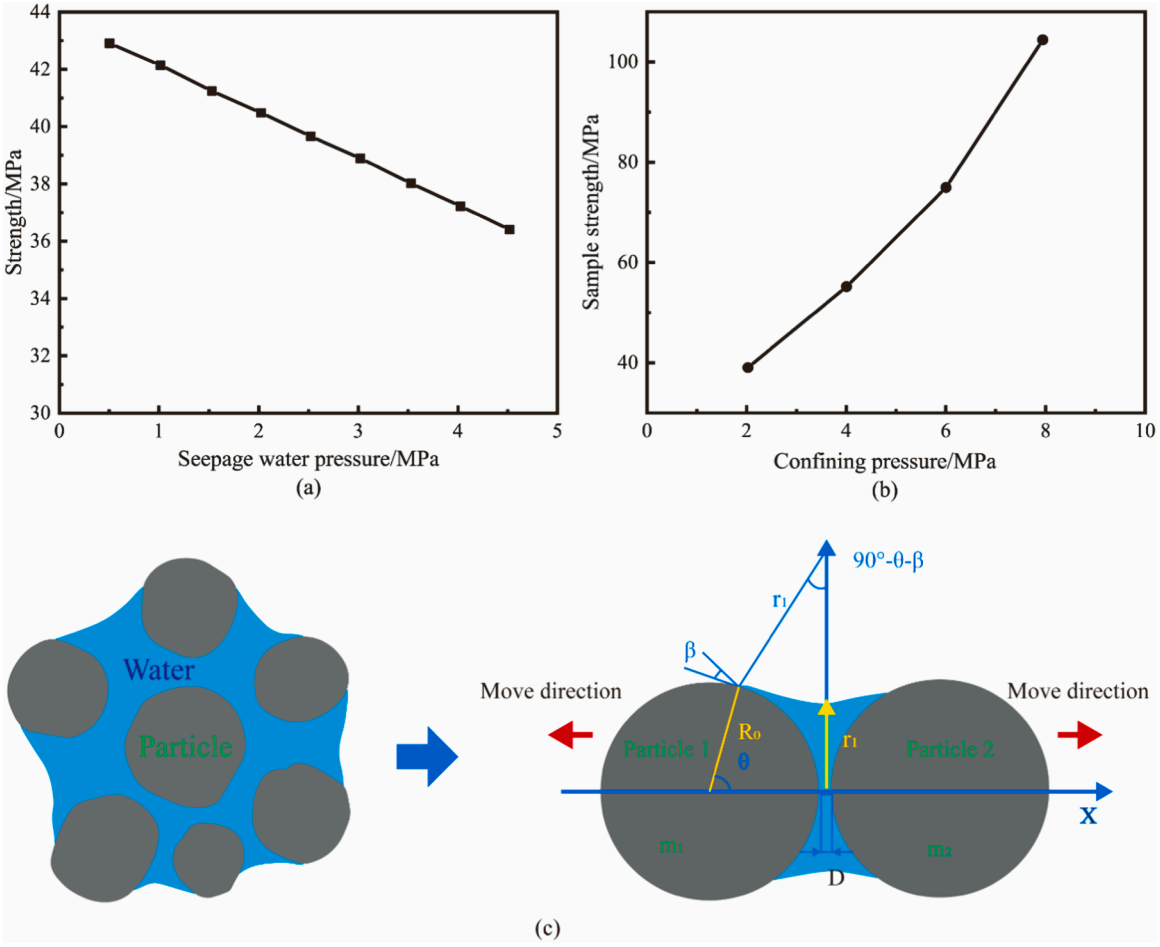

Fig. 19. (a) Relationship between crack initiation strength and seepage water pressure; (b) Relationship between sample strength and confining pressure [149]; (c) Interaction model of the particle-water molecules [150].

because new cracks are produced under the axial preload and the bearing capacity is reduced. With the increase in the axial preload, the shear failure appears gradually in the rock specimen. In addition, the dynamic compressive strength of rocks increases with the hydrostatic pressure, and the failure mode of the specimen changes from tension to shear with the increase in the hydrostatic pressure. Moreover, the effect of the triaxial stress state on the dynamic compressive strength and failure mode of rocks can be considered as the coupling effect of hydrostatic and axial pressure.

The dynamic tensile and shear strength of rocks exhibits significant rate dependence under different hydrostatic pressures and increases with the increase of hydrostatic pressure. The dynamic angle of internal friction is nearly independent of the loading rate. The dynamic tensile strength of rocks decreases with the axial preload, but the total tensile strength remains constant under various axial preloads. This phenomenon is caused by the counteraction of the enhancement of loading rate sensitivity and the weakening induced by the pre-tensile stress in the specimen. The hydrostatic pressure inhibits the crack propagation, thus improving the dynamic tensile strength of rocks. The triaxial stress states can be considered as the combination of the axial preload and the hydrostatic pressure, thus the influence of the triaxial stress on the dynamic tensile strength of rocks can be explained by the mechanisms mentioned in the axial preload and the hydrostatic pressure. In addition, the effect of the axial preload on the dynamic and total flexure strength of rocks is similar to that in the dynamic BD experiment.

The dynamic mode-I and II fracture toughness of rocks exhibit rate dependence under different confining pressures. The dynamic mode-I and II fracture toughness of rocks decreases with the preload while the total mode-I and II fracture toughness of rocks increases with the preload. The dynamic mode-I and II fracture toughness of rocks increases with the increase of confining pressure, whereas the hydrostatic pressure barely influences the dynamic mode-I and II fracture toughness of rocks.

Recently, the coupled hydraulic-mechanical SHPB system for determining the dynamic strength of rocks subjected to the coupled hydraulic-mechanical loading was developed. The dynamic compressive strength of GS increases with the loading rate and the confining pressure but decreases with the pore pressure. In addition, single shear failure and X-type conjugate shear failure are the most common dynamic failure modes under hydrostatic confinement and pore pressure conditions. The cohesion in the Mohr-Coulomb failure criterion is independent of the pore pressure and confining pressure. The free water has a bidirectional effect on the dynamic strength. The influence of pore pressure and differential pore pressure on the dynamic strength is revealed. The permeability of rocks first increases and then decreases with the cyclic impact number. The differential pore pressure enhances the permeability of rocks under the same impact cycle. The main fracture mode of rocks is mainly compressive-shear fracture in combination with a tensile fracture in the middle of the specimen due to the coupling effect of the reflected stress wave and the hydraulic-confining pressure.

In the past few decades, the dynamic tests of deep rocks have extensively been developed and the corresponding experimental results provided significant fundaments for the promising development of deep rock engineering. Although advances in the dynamic test of deep rocks considering in-situ mechanical and hydraulic conditions have recently been achieved, some improvements are necessary to fulfill the function

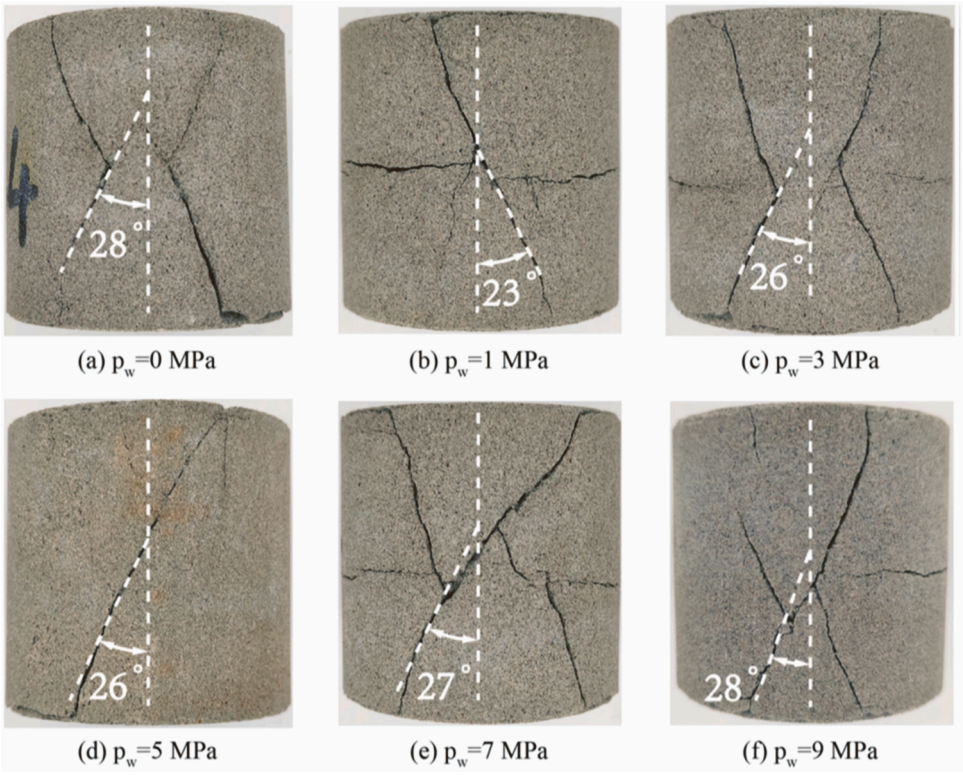

Fig. 20. Failure angle with the pore pressure (Confining pressure = 10 MPa, P_w is pore pressure; Loading rate is about 3094 GPa/s) [146].

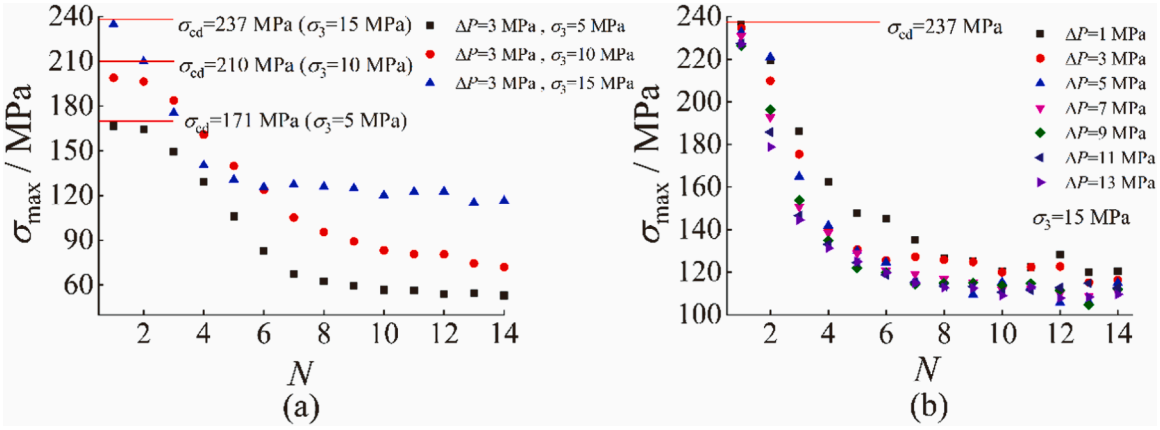

Fig. 21. (a) Evolution of dynamic compressive strength of GS after cyclic impacts under various confining pressures and (b) various differential pore pressures (Note: the red line is the dynamic compressive strength of GS under a certain incident energy.) [147].

for measuring the dynamic behaviors of deep rocks under the true complex geological environment in rock engineering practices. For example, existing dynamic testing techniques can successfully provide both in-situ stress and pore pressure environments for rock specimens, but deep rocks are under high in-situ stress, high pore pressure and high temperature. Consequently, a new dynamic testing system should be developed to simulate the thermal-hydraulic-mechanical coupling environment for deep rocks, and the dynamic mechanical properties of rocks under this coupling condition should be further studied. In addition, another challenge in dynamic tests of deep rock is to compare the on-site data of deep rock engineering with the laboratory experimental data of deep rocks. In such a case, in the future, artificial intelligence methods are expected to be applied in the data analysis of dynamic tests of deep rocks, enhancing the efficiency of data analysis and establishing a bridge between on-site data and laboratory data in deep rock engineering. Therefore, attempts should be made to solve some fundamental technical and scientific issues in dynamic tests of deep rocks under geological occurrence environments.

CRediT authorship contribution statement

Conceptualization: Kaiwen Xia, Wei Yao; Methodology: Kaiwen Xia, Wei Yao, Ying Xu; Formal analysis and investigation: Bangbiao Wu, Ying Xu, Wei Yao, Yan Fu; Writing - original draft preparation: Wei Yao, Minlei Wang, Yan Fu; Writing - review and editing: Kaiwen Xia, Ying Xu, Bangbiao Wu; Funding acquisition: Kaiwen Xia, Ying Xu, Wei Yao, Bangbiao Wu; Resources: Kaiwen Xia

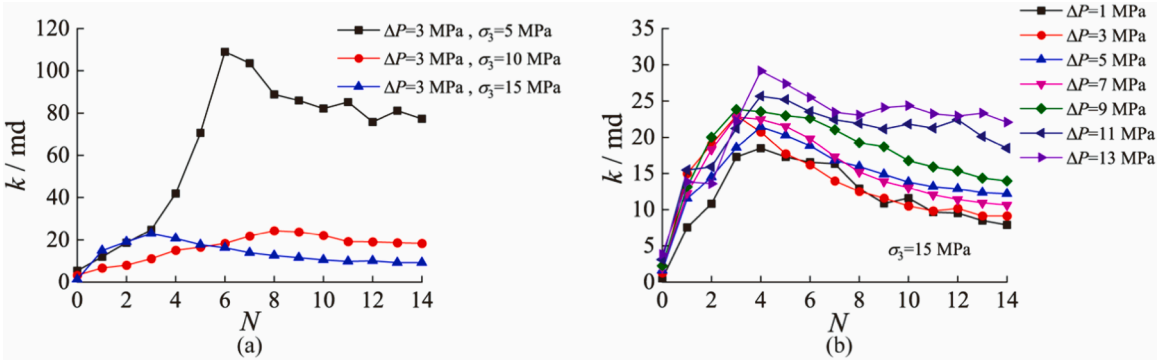

Fig. 22. Evolution of permeability of rock specimens after cyclic impacts with constant input energy under (a) various confining pressures and (b) various differential pore pressures.

Declaration of Competing Interest

The authors declare that they have no known competing financial interests or personal relationships that could have appeared to influence the work reported in this paper.

Acknowledgment

This work was supported by the National Natural Science Foundation of China (Grant Nos. 42141010, 12172253, 42377147, and 52079091).

References

[1] H. Xie, Research review of the state key research development program of china: Deep rock mechanics and mining theory], J. China Coal Soc. 44 (05) (2019) 1283–1305.
[2] C. Wang, G. Gao, S. Yang, Analysis and prediction of stress fields of sichuan—tibet railway area based on contemporary tectonic stress field zoning in western china, Chin. J. Rock. Mech. Eng. 38 (11) (2019) 2242–2253.
[3] Y. Xue, F. Kong, W. Yang, et al., Main unfavorable geological conditions and engineering geological problems along sichuan—tibet railway, Chin. J. Rock. Mech. Eng. 39 (03) (2020) 445–468.
[4] Z. Zheng, Q. Sun, Sichuan—tibet railway tunnel project, Tunn. Constr. 37 (08) (2017) 1049–1054.
[5] W. Chen, H. Huang, P. Ma, Test study of deformation characteristics of deep rock mass in jinping ii hydropower station under ultra-high pressure, Chin. J. Rock. Mech. Eng. 34 (S2) (2015) 3930–3935.
[6] Chen W., Luo H., Jin Y., et al. Deep geological feature of east part in xinchang granite in beishan pre-selected area for the disposal of high-level radio active waste. The Sixth Symposium on Underground Waste Disposal. China, 2016.
[7] X. Wang, D. Li, G. Cheng, et al., Geological disposal of high-level radioactive wastebase to study the structural plane of deep rock mass : a case study of geological disposal of high-level radioactive waste used in the underground research laboratory of gansu beishan area, Geophys. Geochem. Explor. 42 (03) (2018) 481–490.
[8] L. Huang, G. Lu, R. Liu, et al., The application of electromagnetic sounding in deep geothermal investigation, Geophys. Geochem. Explor. (06) (2004) 493–495.
[9] A. Nur, J. Byerlee, An exact effective stress law for elastic deformation of rock with fluids, J. Geophys. Res. (1896-1977) 76 (26) (1971) 6414–6419.
[10] Q. Qian, Challenges faced by underground projects construction safety and countermeasures, Chin. J. Rock. Mech. Eng. 31 (10) (2012) 1945–1956.
[11] H. Zhou, H. Xie, J. Zuo, Research progress of rock mechanical behavior under deep high in-situ stress, Adv. Mech. (01) (2005) 91–99.
[12] H. Xie, F. Gao, Y. Ju, Research and development of rock mechanics in deep ground engineering, Chin. J. Rock. Mech. Eng. 34 (11) (2015) 2161–2178.
[13] S. Zhong, Q. Jiang, X. Feng, et al., A case of in-situ stress measurement in chinese jinping underground laboratory, Rock. Soil Mech. 39 (01) (2018) 356–366.
[14] B. Wu, W. Yao, K. Xia, An experimental study of dynamic tensile failure of rocks subjected to hydrostatic confinement, Rock. Mech. Rock. Eng. 49 (10) (2016) 3855–3864.
[15] K. Liu, Q. Zhang, G. Wu, et al., Dynamic mechanical and fracture behaviour of sandstone under multiaxial loads using a triaxial hopkinson bar, Rock. Mech. Rock. Eng. 52 (7) (2019) 2175–2195.
[16] Q. Zhang, C. Zhou, H. Zhou, et al., Research on rock burst estimation and control measures for auxiliary tunnels in jinping ii hydropower station, Rock. Soil Mech. 30 (S2) (2009) 422–426. +445.
[17] He M., Xie H., Peng S., et al. Study on rock mechanics of deep mining. Research Progress on Soft Rock Engineering and Deep Disaster Control in China—Proceedings of the Fourth Symposium on Deep Rock Mass Mechanics and Engineering Disaster Control and China University of Mining and Technology (Beijing) Centennial Academic Conference, 2005.
[18] Y. Zheng, C. Chen, T. Liu, et al., Numerical study of p-waves propagating across deep rock masses based on the hoek-brown model, Int. J. Geomech. 20 (2) (2020) 9.
[19] X. Li, H. Zhao, Y. Luo, et al., Experimental study of propagation and attenuation of elastic wave in deep rock mass with joints, Chin. J. Rock. Mech. Eng. 34 (11) (2015) 2319–2326.
[20] K. Xia, Y. Xu, R. Chen, Dynamic tests of rocks subjected to simulated deep underground environments, Hazard Control Tunn. Undergr. Eng. 1 (01) (2019) 58–75.
[21] K. Xia, W. Yao, Dynamic mechanical properties of rock under pre-load, Eng. Blasting 21 (06) (2015) 7–13.
[22] M. He, X. Sun, The present situation and prospect of deep rock mechanics and engineering disaster control, 2009—2010 Dev. Rep. Rock. Mech. Rock. Eng. (2010).
[23] He M., Qian Q. Summarize of basic research on rock mechanics and engineering disater control at great depth. Advanced Seminar on Prevention And Control of Sudden Geological Disasters and Disaster Reduction Countermeasures. China, 2006.
[24] K. Xia, Y. W, Dynamic rock tests using split hopkinson (kolsky)bar system - a review, J. Rock. Mech. Geotech. Eng. 7 (1) (2015) 27–59.
[25] Q. Zhang, J. Zhao, A review of dynamic experimental techniques and mechanical behaviour of rock materials, Rock. Mech. Rock. Eng. 47 (4) (2014) 1411–1478.
[26] K. Xia, C. Zhou, Review of testing methods for dynamic rock mechanical properties, Eng. Blastiing 20 (02) (2014) 43–53.
[27] T N, Material behavior at high strain rates, Impact Dyn. (1982) 277–332.
[28] J. Field, S. Walley, W. Proud, et al., Review of experimental techniques for high rate deformation and shock studies, Int. J. Impact Eng. 30 (7) (2004) 725–775.
[29] U. Lindholm, L. Yeakley, High strain-rate testing: tension and compression, Exp. Mech. 8 (1) (1968) 1–9.
[30] R. Christensen, S. Swanson, W. Brown, Split-hopkinson-bar tests on rock under confining pressure, Exp. Mech. 12 (11) (1972) 508–513.
[31] U. Lindholm, L. Yeakley, A. Nagy, The dynamic strength and fracture properties of dresser basalt, Int. J. Rock. Mech. Min. Sci. Geomech. Abstr. 11 (5) (1974) 181–191.
[32] X. Li, Z. Zhou, T. Lok, et al., Innovative testing technique of rock subjected to coupled static and dynamic loads, Int. J. Rock. Mech. Min. Sci. 45 (5) (2008) 739–748.
[33] W. Chen, G. Ravichandran, Failure mode transition in ceramics under dynamic multiaxial compression, Int. J. Fract. 101 (1-2) (2000) 141–159.
[34] D. Frew, S. Akers, W. Chen, et al., Development of a dynamic triaxial kolsky bar, Meas. Sci. Technol. 21 (10) (2010) 10.
[35] Wu B. Dynamic tensile failure of rocks subjected to simulated in situ stresses[M]. 2016.
[36] W. Yao, Y. Xu, K. Xia, et al., Dynamic mode ii fracture toughness of rocks subjected to confining pressure, Rock. Mech. Rock. Eng. 53 (2) (2020) 569–586.
[37] Y. Xu, W. Yao, K. Xia, et al., Experimental study of the dynamic shear response of rocks using a modified punch shear method, Rock. Mech. Rock. Eng. 52 (8) (2019) 2523–2534.
[38] Xu Y., Xia K., Wang S., et al. A split hopkinson pressure bar with an energy absorbing device simulating the in-situ stress environment[P].China, CN201811546962.1, 2018-12-18.
[39] M. Kabir, W. Chen, Dynamic triaxial test on sand, Volume 1, in: T. Proulx (Ed.), Dynamic Behavior of Materials, Springer New York, New York, NY, 2011.
[40] M. Kabir, W. Chen, V.-T. Kuokkala, Measurement of stresses and strains in high rate triaxial experiments, Volume 1, in: T. Proulx (Ed.), Dynamic Behavior of Materials, Springer New York, New York, NY, 2011.
[41] Z. Ye, X. Li, L. Zhou, et al., Static-dynamic coupling strength and deformation characteristics of rock under triaxial compression, Rock. Soil Mech. 30 (07) (2009) 1981–1986.
[42] R. Chen, Experimental studies on mechanicalproperties of a pbx under various dynamicloading conditions[D], National University of Defense Technology, 2011.

[43] S. Nemat-Nasser, J. Isaacs, J. Rome, Triaxial hopkinson techniques. Mechanical Testing and Evaluation, ASM International, 2000.

[44] He M., Qian Q. Summarize of basic research on rock mechanics and engineering disaster control at great depth Advanced Seminar on Prevention And Control of Sudden Geological Disasters and Disaster Reduction Countermeasures. China, 2006.

[45] F. Gong, X. Si, X. Li, et al., Dynamic triaxial compression tests on sandstone at high strain rates and low confining pressures with split hopkinson pressure bar, Int. J. Rock. Mech. Min. Sci. 113 (2019) 211–219.

[46] B. Wu, R. Chen, K. Xia, Dynamic tensile failure of rocks under static pre-tension, Int. J. Rock. Mech. Min. Sci. 80 (2015) 12–18.

[47] W. Yao, K. Xia, T. Zhang, Dynamic fracture test of laurentian granite subjected to hydrostatic pressure, Exp. Mech. 59 (2) (2019) 245–250.

[48] K. Xia, S. Wang, Y. Xu, et al., Advances in experimental studies for deep rock dynamics, Chin. J. Rock. Mech. Eng. 40 (3) (2021) 448–475.

[49] R. Chen, W. Yao, F. Lu, et al., Evaluation of the stress equilibrium condition in axially constrained triaxial shpb tests, Exp. Mech. 58 (3) (2018) 527–531.

[50] China TPSCGOPSRO, Test method for dynamic uniaxial compressive strength of rock materials, Metallurgy Industry Press, Beijing, 2018.

[51] Y. Zhou, K. Xia, X. Li, et al., Suggested methods for determining the dynamic strength parameters and mode-i fracture toughness of rock materials, Int. J. Rock. Mech. Min. Sci. 49 (2012) 105–112.

[52] X. Li, Z. Zhou, T.-S. Lok, et al., Innovative testing technique of rock subjected to coupled static and dynamic loads, Int. J. Rock. Mech. Min. Sci. 45 (5) (2008) 739–748.

[53] Y. Niu, K. Li, D. Liu, et al., Experimental study on impact mechanical properties of red sandstone under one-dimensional stress preloading, J. Exp. Mech. 31 (03) (2016) 409–416.

[54] F. Gong, X. Li, X. Liu, Preliminary experimental study of characteristics of rocksubjected to 3d coupled static and dynamic loads, Chin. J. Rock. Mech. Eng. 30 (06) (2011) 1179–1190.

[55] X. Li, F. Gong, J. Zhao, et al., Test study of impact failure of rock subjected to one dimensional coupled static and dynamic loads, Chin. J. Rock. Mech. Eng. 29 (02) (2010) 251–260.

[56] Z. Yin, X. Li, J. Jin, et al., Failure characteristics of high stress rock induced by impact disturbance under confining pressure unloading, Trans. Nonferrous Met. Soc. China 22 (1) (2012) 175–184.

[57] Z. Zhou, X. Cai, X. Li, et al., Dynamic response and energy evolution of sandstone under coupled static–dynamic compression: insights from experimental study into deep rock engineering applications, Rock. Mech. Rock. Eng. 53 (3) (2020) 1305–1331.

[58] M. Hokka, J. Black, D. Tkalich, et al., Effects of strain rate and confining pressure on the compressive behavior of kuru granite, Int. J. Impact Eng. 91 (2016) 183–193.

[59] F. Gong, X. Li, X. Liu, Preliminary experimenary experimental study of characteristics of rock subjected to 3d coupled static and dynamic loads, J. Rock. Mech. Eng. 30 (06) (2011) 1179–1190.

[60] S. Ma, W. Chen, W. Zhao, Effects of axial static stress and confining pressure on the dynamic compressive behaviours of granite, Eur. J. Environ. Civ. Eng. 25 (5) (2021) 795–812.

[61] D.J. Frew, S.A. Akers, W. Chen, et al., Development of a dynamic triaxial kolsky bar, Meas. Sci. Technol. 21 (10) (2010) 105704.

[62] H. Du, F. Dai, Y. Liu, et al., Dynamic response and failure mechanism of hydrostatically pressurized rocks subjected to high loading rate impacting, Soil Dyn. Earthq. Eng. 129 (2020) 105927.

[63] X. Lu, J. Xu, H. Ge, et al., Effects of confining pressure on mechanical behaviors of sandstone under dynamic impact loads, Chin. J. Rock. Mech. Eng. 29 (01) (2010) 193–201.

[64] E. Li, Y. Tan, C. Ma, et al., Split hopkinson pressure bar test and dynamic strength research of salt rock under three-pressure, Chin. J. Rock. Mech. Eng. 34 (S2) (2015) 3742–3749.

[65] Q. Wang, B. Wu, Y. Guo, Dynamic tensile failure of laurentian granite subjected to triaxial confinement, Geotech. Lett. 9 (2) (2019) 116–120.

[66] Y. Niu, Kunming University of Science and Technology, Exp. Study Mech. Prop. Red. sandstone three-Dimens. Static Stress[D.] (2017).

[67] Z. Zhou, Y. Zhang, A. Yang, et al., Experimental study on mechanical characteristics of dolomite under three-dimensional coupled static-dynamic loading, J. China Coal Soc. 40 (5) (2015) 1030–1036.

[68] X. Li, Z. Zhou, F. Zhao, et al., Mechanical properties of rock under coupled static-dynamic loads, J. Rock. Mech. Geotech. Eng. (2009).

[69] Z. Zhou, Y. Zhang, A. Yang, et al., Experimental study on mechanical characteristics of dolomite under three-dimensional coupled static-dynamic loading, J. China Coal Soc. 40 (05) (2015) 1030–1036.

[70] X. Li, Z. Zhou, F. Zhao, et al., Mechanical properties of rock under coupled static-dynamic loads, J. Rock. Mech. Geotech. Eng. 1 (1) (2009) 41–47.

[71] Y. Niu, K. Li, X. Li, Study of failure mode and mechanical properties of rock subjected to 3d coupled static and dynamic loads, J. Kunming Univ. Sci. Technol. : Nat. Sci. 41 (04) (2016) 33–37. +58.

[72] K. Xia, W. Yao, B. Wu, Dynamic rock tensile strengths of laurentian granite: Experimental observation and micromechanical model, J. Rock. Mech. Geotech. Eng. 9 (1) (2017) 116–124.

[73] F. Dai, K. Xia, S. Luo, Semicircular bend testing with split hopkinson pressure bar for measuring dynamic tensile strength of brittle solids, Rev. Sci. Instrum. 79 (12) (2008) 6.

[74] F. Dai, K. Xia, J. Zuo, et al., Static and dynamic flexural strength anisotropy of barre granite, Rock. Mech. Rock. Eng. 46 (6) (2013) 1589–1602.

[75] China TPSCGOPSRO, Test method for dynamic bending strength of semi-circular bending specimens of rock materials, Metallurgy Industry Press, Beijing, 2018.

[76] Y. Xu, J. Zhang, W. Yao, et al., Experimental study of dynamic fracture energy anisotropy of granitic rocks, Chin. J. Rock. Mech. Eng. 37 (S1) (2018) 3231–3238.

[77] S. Huang, R. Chen, K. Xia, Quantification of dynamic tensile parameters of rocks using a modified kolsky tension bar apparatus, J. Rock. Mech. Geotech. Eng. 2 (2) (2010) 162–168.

[78] S. Liu, H. Li, J. Li, et al., An equipment for dynamic direct tension tests of rock material under confining pressure, Rock. Soil Mech. Mater. (11) (2007) 2365–2368. +2374.

[79] R. Chen, K. Xia, F. Lu, et al., Dynamic tension tests of pre-stressed rocks, Proc. 3th Asia-Pac. Symp. . Blasting Tech. (2011).

[80] Z. Zhou, X. Li, Y. Zou, et al., Dynamic brazilian tests of granite under coupled static and dynamic loads, Rock. Mech. Rock. Eng. 47 (2) (2014) 495–505.

[81] Q. Ping, Z. Fang, D. Ma, et al., Coupled static-dynamic tensile mechanical properties and energy dissipation characteristic of limestone specimen in shpb tests, Adv. Civ. Eng. 2020 (2020) 7172928.

[82] P. Pei, F. Dai, Y. Liu, et al., Dynamic tensile behavior of rocks under static pre-tension using the flattened brazilian disc method, Int. J. Rock. Mech. Min. Sci. 126 (2020) 104208.

[83] W. Yao, K. Xia, A. Jha, Experimental study of dynamic bending failure of laurentian granite: Loading rate and pre-load effects, Can. Geotech. J. 56 (2) (2019) 228–235.

[84] Y. Xu, W. Yao, K. Xia, Numerical study on tensile failures of heterogeneous rocks, J. Rock. Mech. Geotech. Eng. (2019).

[85] W. Yao, K. Xia, X. Li, Non-local failure theory and two-parameter tensile strength model for semi-circular bending tests of granitic rocks, Int. J. Rock. Mech. Min. Sci. 110 (2018) 9–18.

[86] Dai F., Xia K. Rate dependence of tensile/flexural strengths of laurentian granite. 9th International Symposium on Rock Fragmentation by Blasting, FRAGBLAST 9, September 13, 2009 - September 17, 2009. Granada, Spain: CRC Press, 2010.

[87] A. Coviello, R. Lagioia, R. Nova, On the measurement of the tensile strength of soft rocks, Rock. Mech. Rock. Eng. 38 (4) (2005) 251–273.

[88] Y. Xu, W. Yao, K. Xia, Numerical study on tensile failures of heterogeneous rocks, J. Rock. Mech. Geotech. Eng. 12 (01) (2020) 50–58.

[89] Y. Xu, W. Yao, K. Xia, Numerical study on tensile failures of heterogeneous rocks, J. Rock. Mech. Geotech. Eng. 12 (1) (2020) 50–58.

[90] J. Lipkin, K. Schuler, T. Parry, Dynamic torsional failure of limestone tubes. In: ed HJ, ed, 2nd Conf. Mech. Prop. Mater. High. Rates Strain (1979).

[91] J. Lipkin, A. Jones, Dynamic fracture strength of oil shale under torsional loading, Am. Rock. Mech. Assoc. (1979) 1–6.

[92] D. Rittel, S. Lee, G. Ravichandran, A shear-compression specimen for large strain testing, Exp. Mech. 42 (1) (2002) 58–64.

[93] K. Fukui, S. Okubo, A. Ogawa, Some aspects of loading-rate dependency of sanjome andesite strengths, Int. J. Rock. Mech. Min. Sci. 41 (7) (2004) 1215–1219.

[94] S. Huang, X. Feng, K. Xia, A dynamic punch method to quantify the dynamic shear strength of brittle solids, Rev. Sci. Instrum. 82 (5) (2011) 5.

[95] J. Zhao, Applicability of mohr-coulomb and hoek-brown strength criteria to the dynamic strength of brittle rock, Int. J. Rock. Mech. Min. Sci. 37 (7) (2000) 1115–1121.

[96] H. Li, J. Zhao, T. Li, Triaxial compression tests on a granite at different strain rates and confining pressures, Int. J. Rock. Mech. Min. Sci. 36 (8) (1999) 1057–1063.

[97] China TPSCGOPSRO, Test method for dynamic shear strength of punching and shearing specimens of rock materials, Metallurgy Industry Press, Beijing, 2018.

[98] Y. Xu, F. Dai, Dynamic response and failure mechanism of brittle rocks under combined compression-shear loading experiments, Rock. Mech. Rock. Eng. 51 (3) (2018) 747–764.

[99] J. Klepaczko, M. Bassim, T. Hsu, Fracture toughness of coal under quasi-static and impact loading, Eng. Fract. Mech. 19 (2) (1984) 305–316.

[100] C. Tang, X. Xu, A new method for measuring dynamic fracture toughness of rock, Eng. Fract. Mech. 35 (4) (1990) 783–791.

[101] T. Yin, L. Bai, X. Li, et al., Effect of thermal treatment on the mode i fracture toughness of granite under dynamic and static coupling load, Eng. Fract. Mech. 199 (2018) 143–158.

[102] F. Dai, M. Wei, N. Xu, et al., Numerical assessment of the progressive rock fracture mechanism of cracked chevron notched brazilian disc specimens, Rock. Mech. Rock. Eng. 48 (2) (2015) 463–479.

[103] M. Iqbal, B. Mohanty, Experimental calibration of isrm suggested fracture toughness measurement techniques in selected brittle rocks, Rock. Mech. Rock. Eng. 40 (5) (2007) 453–475.

[104] N. Iqbal, B. Mohanty, Experimental calibration of stress intensity factors of the isrm suggested cracked chevron-notched brazilian disc specimen used for determination of mode-i fracture toughness, Int. J. Rock. Mech. Min. Sci. 43 (8) (2006) 1270–1276.

[105] R. Fowell, C. Xu, P. Dowd, An update on the fracture toughness testing methods related to the cracked chevron-notched brazilian disk (ccnbd) specimen, Pure Appl. Geophys. 163 (5-6) (2006) 1047–1057.

[106] R. Fowell, Suggested method for determining mode i fracture toughness using cracked chevron notched brazilian disc (ccnbd) specimens, Int. J. Rock. Mech. Min. Sci. Geomech. Abstr. 32 (1) (1995) 57–64.

[107] F. Dai, K. Xia, H. Zheng, et al., Determination of dynamic rock mode-i fracture parameters using cracked chevron notched semi-circular bend specimen, Eng. Fract. Mech. 78 (15) (2011) 2633–2644.

[108] M. Mostafavi, S. Mcdonald, P. Mummery, et al., Observation and quantification of three-dimensional crack propagation in poly-granular graphite, Eng. Fract. Mech. 110 (2013) 410–420.
[109] Z. Zhang, S. Kou, J. Yu, et al., Effects of loading rate on rock fracture, Int. J. Rock. Mech. Min. Sci. 36 (5) (1999) 597–611.
[110] J. Franklin, Z. Sun, B. Atkinson, et al., Suggest. Methods determining Fract. toughness Rock. (1988).
[111] W. Yao, K. Xia, Dynamic notched semi-circle bend (nscb) method for measuring fracture properties of rocks: Fundamentals and applications, J. Rock. Mech. Geotech. Eng. 11 (5) (2019) 1066–1093.
[112] M. Kuruppu, Y. Obara, M. Ayatollahi, et al., Isrm-suggested method for determining the mode i static fracture toughness using semi-circular bend specimen, Rock. Mech. Rock. Eng. 47 (1) (2014) 267–274.
[113] R. Chen, K. Li, K. Xia, et al., Dynamic fracture properties of rocks subjected to static pre-load using notched semi-circular bend method, Rock. Mech. Rock. Eng. 49 (10) (2016) 3865–3872.
[114] M. Ayatollahi, M. Aliha, On the use of an anti-symmetric four-point bend specimen for mode ii fracture experiments, Fatigue Fract. Eng. Mater. Struct. 34 (11) (2011) 898–907.
[115] M. Li, M. Sakai, Mixed-mode fracture of ceramics in asymmetric four-point bending: Effect of crack-face grain interlocking/bridging, J. Am. Ceram. Soc. 79 (10) (1996) 2718–2726.
[116] Y. Shi, N. Zhou, Comparison of microshear toughness and mode ii fracture toughness for structural steels, Eng. Fract. Mech. 51 (4) (1995) 669–677.
[117] S. Swartz, L. Lu, L. Tang, et al., Mode ii fracture-parameter estimates for concrete from beam specimens, Exp. Mech. 28 (2) (1988) 146–153.
[118] R. Hasanpour, N. Choupani, Rock fracture characterization using the modified arcan test specimen, Int. J. Rock. Mech. Min. Sci. 46 (2) (2009) 346–354.
[119] M. Arcan, Z. Hashin, A. Voloshin, A method to produce uniform plane-stress states with applications to fiber-reinforced materials, Exp. Mech. 18 (4) (1978) 141–146.
[120] H. Azar, N. Choupani, H. Afshin, et al., Effect of mineral admixtures on the mixed-mode (i/ii) fracture characterization of cement mortar: Cts, cstbd and scb specimens, Eng. Fract. Mech. 134 (2015) 20–34.
[121] M. Aliha, R. Pakzad, M. Ayatollahi, Numerical analyses of a cracked straight-through flattened brazilian disk specimen under mixed-mode loading, J. Eng. Mech. 140 (1) (2014) 219–224.
[122] M. Kuruppu, K. Chong, Fracture toughness testing of brittle materials using semi-circular bend (scb) specimen, Eng. Fract. Mech. 91 (2012) 133–150.
[123] Y. Xie, P. Cao, J. Jin, et al., Mixed mode fracture analysis of semi-circular bend (scb) specimen: A numerical study based on extended finite element method, Comput. Geotech. 82 (2017) 157–172.
[124] M. Ayatollahi, M. Aliha, M. Hassani, Mixed mode brittle fracture in pmma - an experimental study using scb specimens, Mater. Sci. Eng. A-Struct. Mater. Prop. Microstruct. Process. 417 (1-2) (2006) 348–356.
[125] S. Chang, C. Lee, S. Jeon, Measurement of rock fracture toughness under modes i and ii and mixed-mode conditions by using disc-type specimens, Eng. Geol. 66 (1-2) (2002) 79–97.
[126] Q. Rao, Z. Sun, O. Stephansson, et al., Shear fracture (mode ii) of brittle rock, Int. J. Rock. Mech. Min. Sci. 40 (3) (2003) 355–375.
[127] B. Lawn. Fracture of brittle solids[M], 2 ed, Cambridge University Press, Cambridge, 1993.
[128] Backers T. Fracture toughness determination and micromechanics of rock under mode i and mode ii loading. 2005.
[129] T. Backers, G. Dresen, E. Rybacki, et al., New data on mode ii fracture toughness of rock from the punch-through shear test, Int. J. Rock. Mech. Min. Sci. 41 (3) (2004) 351–352.
[130] T. Backers, O. Stephansson, E. Rybacki, Rock fracture toughness testing in mode ii - punch-through shear test, Int. J. Rock. Mech. Min. Sci. 39 (6) (2002) 755–769.
[131] T. Backers, O. Stephansson, Isrm suggested method for the determination of mode ii fracture toughness, Rock. Mech. Rock. Eng. 45 (6) (2012) 1011–1022.
[132] J. Watkins, K. Liu, A finite element study of the short beam test specimen under mode ii loading, Int. J. Cem. Compos. Lightweight Concr. 7 (1) (1985) 39–47.
[133] Y. Jung, E. Park, H. Kim, Determination of mode ii toughness of granite by using scc test, ISRM Int. Symp. . - EUROCK 2016 (2016).
[134] Y. Xu, W. Yao, G. Zhao, et al., Evaluation of the short core in compression (scc) method for measuring mode ii fracture toughness of rocks, Eng. Fract. Mech. 224 (2020).
[135] W. Yao, Y. Xu, C.Y. Yu, et al., A dynamic punch-through shear method for determining dynamic mode ii fracture toughness of rocks, Eng. Fract. Mech. 176 (2017) 161–177.
[136] W. Yao, Y. Xu, C. Wang, et al., Dynamic mode ii fracture behavior of rocks under hydrostatic pressure using the short core in compression (scc) method, Int. J. Min. Sci. Technol. 31 (5) (2021) 927–937.
[137] W. Yao, J. Wang, B. Wu, et al., Dynamic mode ii fracture toughness of rocks subjected to various in situ stress conditions, Rock. Mech. Rock. Eng. 56 (3) (2023) 2293–2310.
[138] E. Cadoni, M. Dotta, D. Forni, et al., First application of the 3d-mhb on dynamic compressive behavior of uhpc, EPJ Web Conf. 94 (2015) 01031.
[139] X. Songlin, P. Wang, J. Zhao, et al., Dynamic behavior of concrete under static triaxial loading using 3d-hopkinson bar, Baozha Yu Chongji/Explos. Shock Waves 37 (2017) 180–185.
[140] S. Xu, J. Shan, L. Zhang, et al., Dynamic compression behaviors of concrete under true triaxial confinement: an experimental technique, Mech. Mater. 140 (2020) 103220.
[141] H. Xie, Y. Li, J. Zhao, et al., Temp. Control Syst. Method Hopkins Press. Bar. loaded true triaxial Dyn. Static Comb. (2019).
[142] Xie, H. Zhu, J. Zhou, et al., Novel three-dimensional rock dynamic tests using the true triaxial electromagnetic hopkinson bar system, Rock. Mech. Rock. Eng. 54 (4) (2021) 2079–2086.
[143] M. Chen, S. Xu, L. Yuan, et al., Influence of stress state on dynamic behaviors of concrete under true triaxial confinements, Int. J. Mech. Sci. 253 (2023) 108399.
[144] Xu Y., Xia K., Wang S., et al. A system and method for in-situ seepage measurement of rock materials based on hopkinson bar. 2020.
[145] B. Zou, Z. Luo, F. Xu, et al., Experimental study on impact dynamic characteristics of deep sandstone under thermal-hydraulic-mechanical coupling conditions 39 (9) (2020) 1750–1761.
[146] G. Zhao, X. Li, Y. Xu, et al., A modified triaxial split hopkinson pressure bar (shpb) system for quantifying the dynamic compressive response of porous rocks subjected to coupled hydraulic-mechanical loading, Geomech. Geophys. Geo-Energy Geo-Resour. 8 (1) (2022) 29.
[147] R. Chen, G. Zhao, Y. Xu, et al., Coupled hydraulic-mechanical experimental system for evaluating dynamic mechanical and transport behaviors of deep rocks, Exp. Mech. (2024).
[148] X. Li, X. He, H. Chen, Crack initiation characteristics of opening-mode crack embedded in rock-like material under seepage pressure, Yanshilixue Yu Gongcheng Xuebao/Chin. J. Rock. Mech. Eng. 31 (2012) 1317–1324.
[149] Z. Zhou, P. Cao, Z. Ye, Crack propagation mechanism of compression-shear rock under static-dynamic loading and seepage water pressure, J. Cent. South Univ. 21 (4) (2014) 1565–1570.
[150] K. Wang, G. Feng, J. Bai, et al., Dynamic behaviour and failure mechanism of coal subjected to coupled water-static-dynamic loads, Soil Dyn. Earthq. Eng. 153 (2022) 107084.

Prof. Kaiwen Xia's research is focused on earthquake mechanics, rock dynamics, geological storage of CO2 and safety monitoring of geotechnical engineering. His academic contributions include the discovery of supershear earthquakes in the laboratory, the systematic study of spontaneous fractures and the development of a series of dynamic testing methods for rocks. He has published more than 100 papers in SCI journals, including two first-authored papers published on Science. He was the chair of the Commission on Rock Dynamics of the International Society for Rock Mechanics and Rock Engineering (ISRM). He completed a ISRM suggested dynamic rock testing method and eight Chinese association standards for dynamic testing methods for rocks, which promoted the standardization of the measurement of the dynamic rock properties.

Prof. Wei Yao obtained his PhD from the University of Toronto. He engaged in the research of the dynamic damage and failure mechanism of brittle materials in complex environment, the laboratory earthquake dynamics and CCUS (carbon capture, utilization and storage). He chaired the National Natural Science Foundation of China (NSFC) and participated in editing two industrial standards. He has published more than 50 journal articles, including about 40 SCI journal papers. Dr. Yao's research achievements in rock dynamics and laboratory seismic dynamics can provide theoretical guide for earthquake disaster prevention and deep underground engineering.